Short title: Chemical genetics of auxin-induced Ca^{2+} entry

Corresponding author: Steffen Vanneste
VIB-UGent Center for Plant Systems Biology
Technologiepark 71, 9052 Ghent, Belgium
Tel. +32 33 13844, Fax: +32 9 331 38 09

Title:

Identification of novel inhibitors of auxin-induced Ca^{2+} signaling via a plant-based chemical screen

Authors:

Kjell De Vriese[1,2], Ellie Himschoot[1,2], Kai Dünser[3], Long Nguyen[4,5], Andrzej Drozdzecki[4,5], Alex Costa[6], Moritz K. Nowack[1,2], Jürgen Kleine-Vehn[3], Dominique Audenaert[4,5], Tom Beeckman[1,2] & Steffen Vanneste[1,2,7]

Author Affiliations:

[1]Department of Plant Biotechnology and Bioinformatics, Ghent University, 9052 Ghent, Belgium; [2]VIB Center for Plant Systems Biology, 9052 Gent, Belgium; [3]Department of Applied Genetics and Cell Biology, University of Natural Resources and Life Sciences Vienna (BOKU), 1190 Vienna, Austria; [4]Screening Core, VIB, 9052 Gent, Belgium; [5]Centre for Bioassay Development and Screening (C-BIOS), Ghent University, 9052 Ghent, Belgium; [6]Department of Biosciences, University of Milan, 20133 Milan, Italy; [7]Lab of Plant Growth Analysis, Ghent University Global Campus, 21985 Incheon, Republic of Korea

One-sentence Summary:

Screening of an annotated library of biologically active molecules for inhibitory effects on auxin-induced Ca^{2+} entry in BY-2 cells yielded several new inhibitors for investigating Ca^{2+} signaling.

Footnotes:

Author contributions:

K.D.V., E.H. and K.D. designed and performed the experiments and analyzed the data; A.D. and L.N. provided technical assistance to K.D.V; J.K.V., M.K.N., D.A., T.B. and S.V. supervised the experiments; S.V. and T.B. conceived the project and wrote the article with contributions of all the authors. S.V. agrees to serve as the author responsible for contact and ensures communication.

Funding information:

This work was supported by the Special Research Fund of Ghent University (to K.D.V. and E.H.), Ministero dell'Istruzione dell'Università e della Ricerca, Fondo per gli Investimenti della Ricerca di Base (FIRB) 2010 RBFR10S1LJ_001, University of Milan Transition Grant - Horizon 2020, Fondo di ricerca Linea 1A Progetto "Unimi Partenariati H2020" and Piano di Sviluppo di Ateneo 2016, 2017 (A.C), the Austrian Academy of Sciences (ÖAW) (DOC fellowship to K.D.), Vienna Research Group (VRG) program of the Vienna Science and Technology Fund (WWTF), the Austrian Science Fund (FWF) (Projects: P26568-B16 and P26591-B16), the European Research Council (ERC) (Starting Grant 639478-AuxinER) (to J.K-V.) and the ERC StG PROCELLDEATH (Project Number: 639234) to M.K.N.

Corresponding author email:

stnes@psb.vib-ugent.be

Abstract

Many signal perception mechanisms are connected to Ca^{2+}-based second messenger signaling to modulate specific cellular responses. The well-characterized plant hormone auxin elicits a very rapid Ca^{2+} signal. However, the cellular targets of auxin-induced Ca^{2+} are largely unknown. Here, we screened a biologically annotated chemical library for inhibitors of auxin-induced Ca^{2+} entry in plant cell suspensions to better understand the molecular mechanism of auxin-induced Ca^{2+} and to explore the physiological relevance of Ca^{2+} in auxin signal transduction. Using this approach, we defined a set of diverse, small molecules that interfere with auxin-induced Ca^{2+} entry. Based on annotated biological activities of the hit molecules, we found that auxin-induced Ca^{2+} signaling is, among others, highly sensitive to disruption of membrane proton gradients and the mammalian Ca^{2+} channel inhibitor bepridil. Whereas protonophores nonselectively inhibited auxin-induced and osmotic-stress-induced Ca^{2+} signals, bepridil specifically inhibited auxin-induced Ca^{2+}. We found evidence that bepridil severely alters vacuolar morphology and antagonized auxin-induced vacuolar remodeling. Further exploration of this plant-tailored collection of inhibitors will lead to a better understanding of auxin-induced Ca^{2+} entry and its relevance for auxin responses.

Introduction

The plant hormone auxin is a potent regulator of a diverse set of developmental processes, ranging from embryogenesis, postembryonic organogenesis, and regeneration to tropic growth responses (Vanneste and Friml, 2009). These pluripotent effects in plant development make auxin a key player in the plant's developmental plasticity. Moreover, auxin is subject to extensive cross-talk with many other signaling pathways for flexible integration in auxin-regulated development (Chaiwanon et al., 2016; Liu et al., 2017). Decades of extensive research have led to the formulation of a canonical auxin signaling pathway. In short, the perception of auxin occurs via the auxin-induced stabilization of a coreceptor complex constituted by a TIR1/AFB F-box protein and Aux/IAA proteins, resulting in the ubiquitination and proteolysis of the latter. Consequently, Aux/IAA-interacting AUXIN RESPONSE FACTORs (ARFs) can become active (Lavy and Estelle, 2016; Weijers and Wagner, 2016). This auxin signaling mechanism can explain many of the plant's responses to auxin. In addition, a nontranscriptional branch of TIR1/AFB-based auxin perception was recently connected to the nontranscriptional inhibition of elongation (Fendrych et al., 2018), vacuolar remodeling (Lofke et al., 2015), and activation of Ca^{2+} signaling (Dindas et al., 2018).

A large body of literature describes the role of Ca^{2+} in a variety of cellular processes in plants in the context of responses to light, and biotic and abiotic stress (reviewed in Tuteja and Mahajan, 2007; Kudla et al., 2010; Kudla et al., 2018). However, little is known about the role of Ca^{2+} signaling downstream of auxin. Interestingly, a few reports connect Ca^{2+} to auxin transport regulation (Dela Fuente and Leopold, 1973; Benjamins et al., 2003; Zhang et al., 2011; Rigo et al., 2013). More recently, auxin-induced cytosolic Ca^{2+} increase was proposed to contribute to auxin's inhibitory effect on root growth and auxin-regulated root hair growth via the nonselective cation channel CNGC14 (Shih et al., 2015; Dindas et al., 2018). Jointly, these reports illustrate the importance of Ca^{2+} in auxin physiology. Despite this recent progress, it is clear that much remains to be uncovered about the underlying signaling mechanism and its cellular targets.

Several types of plant Ca^{2+} channel types exist in relatively large gene families, as illustrated in a few examples in Arabidopsis (*Arabidopsis thaliana*): 20 CYCLIC NUCLEOTIDE-GATED CHANNELs (CNGCs; Ma and Berkowitz, 2011), 20 GLUTAMATE RECEPTOR-LIKE CHANNELs (GLRs; Forde and Roberts, 2014), and 16 OSCA/TMEM63 channels (Murthy et al., 2018; Zhang et al., 2018). This genetic complexity greatly hinders pinpointing the Ca^{2+} channels that are involved in a given Ca^{2+} regulated process. Therefore, the involvement of Ca^{2+} in any process in plants is often deduced from using Ca^{2+} chelators such as EGTA and BAPTA or very nonselective Ca^{2+} channel blockers such as La^{3+} and Gd^{3+}. However, these treatments do not reveal anything about the molecular nature of the Ca^{2+} channel involved. Moreover, some important side effects need to be considered when using these treatments to manipulate Ca^{2+}, for example, acidification caused by EGTA and BAPTA releasing four H^+ when binding two Ca^{2+} and the efficient precipitation of phosphates by La^{3+} (reviewed in De Vriese et al., 2018).

The importance of Ca^{2+} in human physiology and neurology led to the development of an extensive pharmacological toolbox to manipulate specific groups of Ca^{2+} channels. Simple drug treatments thus allow manipulation of specific Ca^{2+} channels and evaluation of its effect on any process of interest. Unfortunately, the Ca^{2+} signaling machinery in plants has diverged significantly from the one in the animal kingdom, with many of the Ca^{2+} signaling components of animals being absent in plants and *vice versa* (Nagata et al., 2004; Edel et al., 2017). For instance, channels associated with muscle and nerve Ca^{2+} signal transduction in animals, such as L-type voltage-dependent Ca^{2+} channels (VDCCs; Zuccotti et al., 2011), inositol 1,4,5-triphosphate receptors (IP_3Rs; Nixon et al., 1994), and ryanodine receptors (RyRs; Lanner et al., 2010) are either missing or significantly different in plants. Hence, many Ca^{2+} channel inhibitors established in animal systems are arguably of limited use in plants. Only a few ionotropic GLR inhibitors (DNQX, CNQX, MNQX, and AP5) were also shown to have inhibitory effects on specific plant GLR-based Ca^{2+} channeling activities (reviewed in De Vriese et al., 2018), but the molecular nature and specificity of these inhibitory effects

remain to be characterized. These examples illustrate that there is an important need to develop Ca^{2+} channel inhibitors directly in plant systems to stimulate plant Ca^{2+} research.

Here, we set out to identify small molecules that modify the shape and amplitude of auxin-induced cytosolic Ca^{2+} dynamics and use them to further explore the role of Ca^{2+} signaling in cellular auxin responses. We screened a collection of biologically active and structurally diverse compounds for inhibitors of auxin-induced Ca^{2+} signaling in transgenic tobacco (*Nicotiana tabacum*) BY-2 cell lines that express YFP-apoaequorin as a reporter of Ca^{2+} signaling. Our primary screen identified 80 potential inhibitors, of which 67 were reconfirmed in a confirmation screen. Based on annotated biological functions, we found that protonophores nonselectively interfered with auxin-induced Ca^{2+}. Moreover, we found that auxin-induced Ca^{2+} signals were much more sensitive to bepridil than hyperosmotic-stress-induced Ca^{2+} signals. This differential drug sensitivity is consistent with distinct Ca^{2+} channel types being involved in the Ca^{2+} response (Yuan et al., 2014; Shih et al., 2015; Dindas et al., 2018). Interestingly, we found that bepridil had a severe impact on vacuolar morphology, to the extent that it antagonized auxin-induced vacuolar remodeling. The resulting set of inhibitors thus represents a valuable expansion of the toolbox with nonspecific and semiselective inhibitors for exploring the role of Ca^{2+} signaling in plants.

Results

Assay development and chemical screen

Unlike whole plants, which are composed of complex mixtures of cell types with different stimulus sensitivities, tobacco BY-2 cell suspension cultures are highly homogenous in terms of cell type and developmental stage, thus making them highly suited for high-throughput screening in a multiwell format. A BY-2 cell suspension line expressing YFP-fused apoaequorin (YA) (Mehlmer et al., 2012) was established for luminescence-based quantification of Ca^{2+} signals (Shimomura et al., 1962; Knight et al., 1991). Aequorin is a

bioluminescent photoprotein that emits blue light upon Ca^{2+} binding and has been used extensively as a Ca^{2+} sensor (Shimomura et al., 1962; Shimomura, 2005) (Fig. 1A). The YFP fused to the aequorin was used to visualize expression of the probe in the BY-2 cells but did not contribute to the sensor activity. The assay was miniaturized to 96-well plate format and validated by assessing the effect of 14 known elicitors of Ca^{2+} signaling. The known elicitors induced distinct signals in this BY-2 cell culture (Fig. 1B-O), corroborating the suitability of the cells to assess the effect on Ca^{2+} signaling.

The BY-2 cell suspensions were poorly responsive to exogenous application of auxins (Fig. 1H-J). This probably reflects an auxin insensitivity that is associated with prolonged culturing of the cells in relatively high 2,4-D concentrations (0.2 mg/L ≈ 1 µM in the growth medium). Therefore, the 2,4-D concentration was increased to 500 µM, which resulted in a robust auxin-induced Ca^{2+} response. Immediately after 2,4-D addition, the luminescent signal rapidly increased and reached a maximum after approximately 90 seconds, which attenuated to close to baseline levels around 300 seconds after addition (Fig. 1J). By using the viability stains propidium iodide (PI) and fluorescein diacetate (FDA), no obvious difference in cellular integrity was observed after 1-hour treatment with 2,4-D, suggesting that the immediate Ca^{2+} response to 2,4-D (within minutes) is unlikely the result of a defect in cellular viability (Supplemental Fig. S1).

Next, we aimed to evaluate the quality of our assay by calculating its Z-prime (Z') factor, which is a commonly used statistical indicator of quality for high-throughput assays (Zhang et al., 1999). It allows estimation of the quality of the bioassay in discriminating the effect of hit molecules from read-out variation based on two parameters: 1) the 'separation band' of the assay: the difference between the mean of the negative control plus three times the standard deviations of the negative control and the mean of positive control minus three times the standard deviations of the positive controls, and 2) the dynamic range of the assay: the difference between the mean of the positive and negative controls. In a good assay, the means of the positive and negative controls differ strongly from each other, while the

178 standard deviations are very low (Fig. 2A). An ideal assay has a Z' factor close to 1, and
179 assays with a Z' factor between 0.5 and 1 are generally considered to be excellent (Zhang et
180 al., 1999). Here, we calculated the Z' value of our assay based on the means and standard
181 deviations of the peak intensities of mock-treated cells (DMSO) and cells treated with a
182 nonspecific Ca^{2+} channel inhibitor ($GdCl_3$) (Fig. 2A). The Z' factor was 0.54, suggesting that
183 our assay is robust enough to reliably distinguish potential inhibitors from well-to-well
184 variation. Subsequently, we used this experimental setup to screen the Spectrum collection
185 (MicroSource Discovery Systems) of 2,320 annotated compounds (Fig. 2B). This resulted in
186 the identification of 80 molecules that reduced the maximal response induced by 500 µM 2,4-
187 D to less than 55% of that of the respective DMSO controls. Next, we used a more sensitive
188 well-per-well reconfirmation assay via a plate reader, which also allowed assay of the viability
189 of the cells at the end of the assay by adding a discharge solution. This treatment causes
190 disruption of the membrane integrity and flooding of the cytoplasm with Ca^{2+}, which binds the
191 remnant reconstituted aequorin, and thus generates a sharp, strong luminescence peak
192 (discharge peak) (Fig. 2C). Out of the 80 primary hits, 67 were reconfirmed for reducing the
193 auxin-responsive Ca^{2+} signal by more than 45% (Supplemental Table S1). Of these 67
194 confirmed hits, 39 showed no obvious short-term cytotoxicity, as evidenced by the presence
195 of a large Ca^{2+} discharge peak (Fig. 2C (green); Supplemental Table S1 (confirmed)).
196 However, 28 confirmed hits caused a reduction (Fig. 2C (yellow); Supplemental Table S1
197 (semi-confirmed)) or even complete absence of the Ca^{2+} discharge peak, indicating a defect
198 in Ca^{2+} compartmentalization mechanisms and/or cell viability (Fig. 2C (blue); Supplemental
199 Table S1 (cytotoxic)). Based on structural features, the 67 hits retained after the confirmation
200 screen could be organized into 43 clusters of structurally similar compounds (Supplemental
201 Table S1).

202 Given that both the primary screen and confirmation screen represented single-well
203 analyses, we aimed to further validate a part of our dataset using multiple biological repeats.
204 Therefore, we selected 13 commercially available hit molecules representing a large

chemical diversity for further validation (Table 1). The auxin-induced Ca^{2+} responses were analyzed in 4-8 replicates on YFP-apoaequorin-expressing BY-2 cells (Mehlmer et al., 2012). Out of the 13 tested chemicals, 10 could be confirmed to strongly modify the 2,4-D induced Ca^{2+} signature, while maintaining a robust discharge peak (Fig. 2D). Together, these data highlight that our set of 67 hits after the confirmation screen is rich in potent modifiers of auxin-induced Ca^{2+} signaling.

Fenamates alter the shape of auxin-induced Ca^{2+}

Among the 67 confirmed hit compounds, we found four highly related fenamate-type chemicals: flufenamic acid (FFA **(1)**), niflumic acid (NFA **(2)**), tolfenamic acid (TFA **(3)**), and flunixin meglumine **(4)** (structures of all compounds described in the manuscript are shown in Supplemental Fig. S2). Unlike any other tested hit compounds, which simply reduced the amplitude of the Ca^{2+} response, these fenamates had a dramatic effect on the shape of the Ca^{2+} response. Treatment with FFA, NFA, or TFA reduced the maximum of the Ca^{2+} signal, but also revealed a novel Ca^{2+} signal that preceded the maximum (Fig. 3A-C). Such an effect on the Ca^{2+} signal shape was not observed for any of the other hit compounds that were selected for validation.

Seedlings grown for 7 days in the presence of 20 µM FFA, NFA, or TFA had significantly shorter roots than seedlings grown on control plates and displayed a reduced gravitropic root growth, as indicated by a reduced vertical growth index (Fig. 3D-E; Supplemental Fig. S3). Consistently, we observed spreading of the expression of the synthetic auxin response reporter DR5rev::VENUS-N7 in the columella and stem cell niche (Fig. 3F-H), reminiscent of an inhibitory effect on auxin transport. However, neither of the two known auxin transport inhibitors, 2-[4-(diethylamino)-2-hydroxybenzoyl]benzoic acid (BUM **(8)**) and 1-N-naphtylphtalamic acid (NPA **(9)**), had an obvious effect on auxin-induced Ca^{2+} (Fig. 4A-C),

suggesting that a block in auxin transport does not explain the effect of fenamates on Ca^{2+} signaling.

The inhibition of cyclooxygenase activity by fenamates renders them suitable for use as nonsteroidal anti-inflammatory drugs (NSAIDs) (Graham, 2016), and NFA has reported anion channel inhibitory activities (Diatloff et al., 2004; Gilliham and Tester, 2005). Based on these reported bioactivities, we investigated whether other NSAIDs and anion channel inhibitors have a similar effect on Ca^{2+} signaling (Fig. 4A). Of two structurally unrelated NSAIDs (ibuprofen **(10)** and oxaprozin **(11)**) and two unrelated anion channel inhibitors, 5-nitro-2-(3-phenylpropylamino) benzoic acid (NPPB **(12)**) and 9-anthracenecarboxylic acid (9-ACA **(13)**), only NPPB inhibited auxin-induced Ca^{2+} (Fig. 4D-G). However, the effect of NPPB was clearly distinct from the effect of fenamates on Ca^{2+} response dynamics (Fig. 4G), suggesting that the observed effects of fenamates on Ca^{2+} signaling are independent of any additional effects on cyclooxygenases or anion channels.

These analyses suggest that the effect of fenamates on Ca^{2+} signaling is not related to any of their known (cyclooxygenase inhibition and anion channel inhibition) and observed (auxin transport inhibition) biological activities but is rather a distinct feature associated with the chemical structure. Therefore, we also tested the effect of a range of commercially available structurally similar compounds to see whether the effect of the fenamates could be explained by the presence of a specific substructure (Fig. 4A). However, every tested molecular variant (diphenylamine **(14)**, diphenylmethane **(15)**, α-phenyl-o-toluic acid **(16)**, aniline **(17)**, and anthranilic acid **(18)**) failed to inhibit/modify auxin-induced Ca^{2+} signals at 50 µM (Fig. 4H-L), suggesting that the fenamate-core structure represents the biological activity on Ca^{2+}. Moreover, when revisiting the primary screen data of all fenamates that were included in the Spectrum library, we found that fenamic acid **(5)** and mefenamic acid **(6)** showed a tendency to reduce the Ca^{2+} response changes, albeit with a lower potency than the validated fenamates, while the effect of meclofenamate sodium **(7)** was negligible (Fig. 4A).

When we evaluated the 2,4-D-sensitive root growth, no obvious resistance or hypersensitivity could be observed, suggesting that fenamates do not affect auxin perception or 2,4-D uptake (Supplemental Fig. S4A). Similarly, no obvious resistance or hypersensitivity to the ethylene precursor 1-aminocyclopropane-1-carboxylic acid (ACC) could be observed in seedlings grown in the presence of these fenamates (Supplemental Fig. S4A). In addition, we also evaluated the effects of NPPB, 9-ACA, BUM, NPA, and the fenamate analogues on root growth and their sensitivity to 2,4-D and ACC (Supplemental Fig. S4B). Interestingly, unlike FFA, NFA, and TFA, diphenylamine, aniline, and anthranilic acid caused a significant 2,4-D resistance, which further illustrates a completely different mode of action between the effective fenamates and diphenylamine, aniline, and anthranilic acid.

Protonophores impair the Ca^{2+} response to distinct stimuli and render roots insensitive to 2,4-D

Inspection of the 67 confirmed hits revealed a total of at least 13 molecules with reported protonophore activities in different organisms (Supplemental Table S1), suggesting an important contribution of H^+ gradients to auxin-induced Ca^{2+}. We selected niclosamide **(19)**, (+)-usnic acid **(20)**, and cloxyquin **(21)** as structurally diverse representatives of this group of hits. Both niclosamide and (+)-usnic acid could be confirmed as potent inhibitors of auxin-induced Ca^{2+} signals (Fig. 5A-B), while cloxyquin only caused a modest reduction in the peak of the Ca^{2+} signal (Fig. 5C). To test whether the suspected protonophore activities of niclosamide and (+)-usnic acid are the underlying cause of their observed inhibitory effect on Ca^{2+} signals, we also analyzed three well-characterized, but structurally unrelated protonophores: carbonyl cyanide m-chlorophenyl hydrazone (CCCP **(22)**), tyrphostin A23 (TyrA23 **(23)**) and endosidin9 (ES9 **(24)**) (Dejonghe et al., 2016). In addition, we included the K^+ selective ionophore valinomycin **(25)** to account for general disruption of gradients of monovalent cations. Similar to niclosamide and (+)-usnic acid, the three tested

283 protonophores were potent inhibitors of 2,4-D-induced Ca^{2+} signaling (Fig. 5D). Importantly,
284 protonophore treatment did not have obvious defects in Ca^{2+} discharge profiles in the BY-2
285 cells, suggesting that an impaired Ca^{2+} compartmentalization cannot explain the inhibition of
286 2,4-D-induced Ca^{2+}. Unlike the protonophores, valinomycin did not reduce the maximal Ca^{2+}
287 responses (Fig. 5D), suggesting that 2,4-D-induced Ca^{2+} signaling specifically requires
288 proton-based gradients, rather than K^+ gradients. These findings are entirely consistent with
289 the recently reported very tight interdependence between H^+ and Ca^{2+} dynamics (Behera et
290 al., 2018).

291 Because protonophores dissipate H^+-gradients across membranes, including the
292 mitochondrial membranes, they are expected to interfere with ATP production due to
293 mitochondrial uncoupling. Therefore, we evaluated the evolution of ATP content in BY-2 cells
294 during 60-minute treatments with 20 or 50 µM niclosamide, (+)-usnic acid, or cloxyquin (Fig.
295 5E). As a positive control we included the well-described protonophore CCCP (20 µM).
296 Within 2 minutes, niclosamide, (+)-usnic acid, and CCCP caused a significant reduction of
297 cellular ATP levels compared to DMSO-treated cells. Niclosamide had a milder effect on the
298 ATP levels than (+)-usnic acid and CCCP. In contrast, cloxyquin did not interfere with ATP
299 production, even at prolonged incubation times. This suggests that niclosamide and (+)-usnic
300 acid have protonophore activities in plants, which could explain how they inhibit 2,4-D-
301 induced Ca^{2+} signals.

302 Next, we evaluated the effects of these molecules on root growth (Fig. 5F). While cloxyquin
303 did not cause any noticeable defects, plants treated with niclosamide had on average slightly
304 longer primary roots, while (+)-usnic acid had a strong inhibitory effect on the primary root
305 length, suggesting that they have distinct cellular targets. Moreover, (+)-usnic acid induced
306 DR5rev::VENUS-N7 expression in the lateral root cap, which was not observed with
307 niclosamide and cloxyquin (Fig. 5G-J). When cotreated with 100 nM 2,4-D and niclosamide
308 or cloxyquin (but not (+)-usnic acid), the seedlings had significantly longer roots than the
309 controls (Fig. 5F). However, as cloxyquin only caused a slight inhibition of 2,4-D-induced

Ca^{2+} signaling and did not disturb ATP production in BY-2 cells, the observed resistance to 2,4-D is likely unrelated to impairment of Ca^{2+} signaling or protonophore activity. Importantly, the protonophores did not render root growth resistant to ACC (Fig. 5F), as seen for 2,4-D uptake-defective *aux1* mutants (Swarup et al., 2001), suggesting that the observed 2,4-D resistance is not due to impaired AUX1-mediated auxin uptake.

Bepridil is a potent inhibitor of auxin-induced Ca^{2+} signaling and modifies vacuolar morphology

Bepridil **(26)** is the only molecule inhibitor with reported Ca^{2+} channel inhibitory effects that we identified in our chemical screen (Yatani et al., 1986; Sarajarvi et al., 2012; Lipsanen et al., 2013). Also, in the validation, bepridil robustly interfered with the auxin-induced Ca^{2+} response compared to mock-treated cells, while maintaining a strong response to the discharge solution (Fig. 6A). This suggests that bepridil is a potent inhibitor of 2,4-D-induced Ca^{2+} signaling in BY-2 cells. Moreover, bepridil potently inhibited the rapid IAA-induced Ca^{2+} response in roots of Arabidopsis seedlings expressing the intensiometric Ca^{2+} sensor R-GECO1 (Fig. 6B-C; Supplemental Video S1).

Bepridil treatment on Arabidopsis seedlings caused a dose-dependent reduction in primary root length (Fig. 6D), which was associated with altered DR5rev::VENUS-N7 expression in the lateral root cap (Fig. 6E-F). Cotreatment of seedlings with 20 µM bepridil and either 100 nM 2,4-D, 20 µM ACC, 150 nM NAA, or 250 nM NAA did not result in noticeable growth resistance to any of the hormone treatments (Fig. 6G). Because vacuolar remodeling was proposed to be part of the mechanism by which auxin inhibits root growth (Löfke et al., 2015) and because bepridil interferes with auxin-induced Ca^{2+} signaling, we next investigated the effect of bepridil on vacuoles by analyzing the localization of the tonoplast marker VAMP711-YFP (Fig. 6H-I). Bepridil dramatically altered vacuolar morphology, inducing swollen and roundish central vacuoles in Arabidopsis roots (Fig. 6H). Notably, auxin treatments induce

smaller luminal vacuoles, which consequently impact on cellular elongation rates (Löfke et al., 2015; Scheuring et al., 2016). However, in the presence of bepridil, the auxin effect on vacuolar morphology was abolished (Fig. 6H-I), tentatively suggesting that auxin-regulated vacuolar remodeling could depend on a bepridil-sensitive step.

During the vacuolar morphology experiments, the tonoplast marker VAMP711-YFP seemed to display some ectopic subcellular pattern. Therefore, we also analyzed several fluorescent, late endosomal markers. Each of these markers had an aberrant localization pattern after bepridil treatment (Supplemental Fig. S5). These observations suggest that bepridil has pleiotropic effects on late endosomal trafficking, which could complicate the interpretation of the auxin resistance of vacuolar remodeling after bepridil treatment. When lowering the bepridil concentration, we found that vacuolar morphology was still aberrant at 10 µM, but was no longer obviously impaired at 5 µM (Supplemental Fig. S6).

Sucrose-induced Ca^{2+} signals are highly sensitive to fenamates and sterol biosynthesis inhibitors, but not to bepridil

Next, we sought to evaluate the specificities of the identified inhibitors. The auxin response requires CNGC14 for eliciting Ca^{2+} (Shih et al., 2015; Dindas et al., 2018), while hyperosmotic stress is predicted to activate OSCA/TMEM63-type mechanosensitive Ca^{2+}-permeable channels (Yuan et al., 2014; Murthy et al., 2018; Zhang et al., 2018). Thus, auxin and hyperosmotic stress activate two distinct Ca^{2+} entry mechanisms.

We used 0.5 M sucrose as a hyperosmotic stimulus. When eliciting YFP-apoaequorin-expressing Arabidopsis seedlings, we observed a very fast and transient rise in $[Ca^{2+}]_{cyt}$ (Fig. 7; Supplemental Fig. S7), as was previously described for such hyperosmotic treatments (Furuichi et al., 2001; Stephan et al., 2016). The sucrose-induced Ca^{2+} signal was characterized by an initial large peak in free $[Ca^{2+}]_{cyt}$ that reached a maximum value (1.5-2 µM range) within seconds. After reaching the maximum peak value, the Ca^{2+} signal quickly

decreased until it reached an elevated steady-state concentration 30-40 seconds after elicitor addition (Fig. 7; Supplemental Fig. S7).

We evaluated the fenamates (FFA, NFA, and TFA), the protonophores (niclosamide, (+)-usnic acid, ES9, and CCCP), and bepridil for their ability to inhibit hyperosmotic-stress-induced Ca^{2+}. Additionally, we also tested two imidazole-type fungicides (clotrimazole **(27)** and oxiconazole nitrate **(28)**), which were initially identified as inhibitors of 2,4-D-induced Ca^{2+} signals but were not further pursued in the context of auxin responses due to a poor reproducibility in follow-up experiments (Supplemental Fig. S8). All tested fenamates, three protonophores ((+)-usnic acid, ES9, and CCCP) and, surprisingly, both imidazoles potently interfered with sucrose-induced Ca^{2+} (Fig. 7; Supplemental Fig. S7). This suggests that hyperosmotic stress Ca^{2+} entry is much more sensitive to inhibition of sterol biosynthesis than 2,4-D-induced Ca^{2+} responses. On the other hand, while bepridil and niclosamide were potent inhibitors of auxin-induced Ca^{2+}, they did not inhibit the sucrose-induced Ca^{2+} response (Fig. 7D, H). Niclosamide was the only one of the tested protonophores that could not inhibit sucrose-induced Ca^{2+}, suggesting that its inhibitory effect on auxin-induced Ca^{2+} may not be related solely to its protonophore activity. Together, these data illustrate that auxin and hyperosmotic stress Ca^{2+} responses show different pharmacological sensitivities.

Discussion

The molecular mechanism by which auxin regulates transcriptional changes is largely captured by the very well characterized TIR1/AFB-based degradation of Aux/IAA transcriptional corepressors. This pathway accounts for much of the auxin-regulated transcriptional changes and, thus, the cellular response. Recently, TIR1/AFB-based auxin perception was also found to be required for nontranscriptional cellular responses, such as rapid and reversible inhibition of root growth (Fendrych et al., 2018). The inhibitory effect of auxin root elongation is correlated with alkalinization of the apoplast (Barbez et al., 2017),

activation of Ca^{2+} signals through CNCG14 (Shih et al., 2015), and remodeling of the vacuole (Löfke et al., 2015). Alkalinization of the apoplast is possibly the result of the coordinated inhibition of plasma membrane H^+-ATPase activity and AUX1-mediated H^+/IAA^- uptake from the apoplast (Dindas et al., 2018). Moreover, auxin-induced alkalinization of the apoplast is coupled to CNGC14-dependent auxin-induced Ca^{2+} signaling in the epidermis (Shih et al., 2015). Importantly, root elongation of *cngc14* mutants is mildly insensitive to inhibitory auxin levels (Shih et al., 2015), suggesting that auxin-induced cytosolic Ca^{2+} increase is part of the root growth inhibitory auxin signaling pathway. We identified bepridil as a potent inhibitor of auxin-induced cytosolic Ca^{2+} increase and found that bepridil interferes strongly with auxin-induced vacuolar remodeling. This makes it tempting to speculate that auxin-induced cytosolic Ca^{2+} increase controls vacuolar morphology. However, the strong pleiotropic effects on late endosomal compartments preclude drawing such strong conclusions. Therefore, it will be interesting to identify the molecular target(s) of bepridil and characterize its function in auxin-regulated vacuolar remodeling.

The identification of bepridil as a potent inhibitor of auxin-induced Ca^{2+} is consistent with its reported Ca^{2+} channel blocker function in animals (Yatani et al., 1986; Sarajarvi et al., 2012; Lipsanen et al., 2013) and suggests, in line with *cngc14*'s defects in auxin-induced cytosolic Ca^{2+} increase (Shih et al., 2015), that CNGC14 might be a bepridil target. However, electrophysiological experiments demonstrated that bepridil inhibits outward rectified K^+ currents in plant protoplasts (Thomine et al., 1994). This hints at a functional coupling of auxin-induced Ca^{2+} entry with outward rectified K^+ currents as described for Ca^{2+} spiking during nodulation (Ane et al., 2004; Charpentier et al., 2008; Charpentier et al., 2016). However, auxin activates inward rectified K^+ currents in Arabidopsis and maize (Thiel and Weise, 1999; Philippar et al., 2004), and we found that the K^+ selective ionophore valinomycin had no effect on auxin-induced Ca^{2+} signals. Instead, it seems more likely that bepridil targets CNGC14 and/or other CNGCs via structural features that they share with outward rectifying K^+ channels.

Recently, the protonophore carbonyl cyanide-4-(trifluoromethoxy) phenylhydrazone (FCCP) was shown to completely inhibit the ATP-induced Ca^{2+} response, while pretreatment with the ionophore nigericin only had marginal effects on the Ca^{2+} and pH transients (Behera et al., 2018). These observations are perfectly in line with our findings showing that protonophores are potent inhibitors of auxin- and osmotic-stress-induced Ca^{2+} signaling and strengthen previous notions that Ca^{2+} and pH are functionally coupled in several cellular processes in plants, including root hair and pollen tube growth (Herrmann and Felle, 1995; Monshausen et al., 2008; Michard et al., 2017), cold stress response (Gao et al., 2004), and touch response (Monshausen et al., 2009). Also, disruption of the transmembrane pH gradient via alkalinization of the apoplast interfered with auxin-induced Ca^{2+} entry in root hairs (Dindas et al., 2018). This was explained by a need for a proton gradient to drive AUX1-mediated H^+/IAA^- symport into the cell. In this model, the inability of IAA to enter the cell in *aux1* prevents TIR1-mediated CNGC14 activation (Dindas et al., 2018). In turn, *cngc14* has a defect in AUX1 activity, providing a mechanistic model for the coupling of Ca^{2+} and H^+ dynamics during auxin response. However, NAA-induced cytosolic Ca^{2+} increase was recently also coupled to a cytoplasmic acidification (Behera et al., 2018), which cannot be explained by AUX1-mediated H^+ uptake, as NAA is not a good substrate for AUX1 (Yang et al., 2006).

In summary, by exploring a small subset of hits, we readily identified several new inhibitors of auxin-induced Ca^{2+}. Further exploration of these inhibitors will thus lead to novel insights in the mechanism (e.g. protonophores) and the physiological relevance of auxin-induced Ca^{2+} (e.g. vacuolar remodeling). Importantly, the use of a library of annotated molecules has the added advantage that many of the compounds are commercially available and thus are easily accessible to researchers for further characterization and analysis of structural derivatives with a higher inhibitory potency and specificity. Identification of the molecular targets will be key for further refining the inhibitors in terms of specificity and affinity.

Materials and methods

BY-2 cell lines and Arabidopsis plant lines

We stably transformed wild-type tobacco BY-2 (*Nicotiana tabacum* L. cv. Bright Yellow 2) cell suspensions with a kanamycin-resistant construct for constitutive expression of YFP-fused apoaequorin (AEQ) driven by an ubiquitin (UBQ10) promoter as previously described (Mehlmer et al., 2012). The transgenic BY-2 cell lines were maintained by weekly dilution (1:40) in modified Linsmaier and Skoog (LS) medium. The cell cultures were agitated on a rotary shaker at 130 rpm at 25°C in the dark and used in experiments 5 days after subculture.

Transgenic Col-0 Arabidopsis seedlings that carry a proUBQ10::YFP-apoAEQ cassette were used in our experiments (Mehlmer et al., 2012). These lines were generated using *Agrobacterium*-mediated transformation via the floral-dip method (Clough and Bent, 1998). Transformants were selected based on BASTA resistance and YFP expression levels and were made homozygous in subsequent generations.

The other used plant lines expressing R-GECO1 (Keinath et al., 2015), DR5rev::VENUS-N7 (Heisler et al., 2005), Ara7-mRFP (Jia et al., 2013), VAMP727-YFP (Ebine et al., 2008), 2xFYVE-YFP (Vermeer et al., 2006), VAMP711-YFP (Geldner et al., 2009), VAMP711-mCherry (Geldner et al., 2009)have been described previously.

Compounds

The compounds used for the primary screen and confirmation screen belong to the Spectrum compound library (MicroSource Discovery Systems) and were dissolved in DMSO. The compounds used in follow-up experiments (FFA, NFA, TFA, diphenylamine, diphenylmethane, α-phenyl-o-toluic acid, aniline, anthranilic acid, NPPB, 9-ACA, NPA, BUM, clotrimazole, oxiconazole nitrate, artemether, niclosamide, (+)-usnic acid, cloxyquin, bepridil,

TyrA23, CCCP, and valinomycin) were obtained from Sigma-Aldrich (Overijse, Belgium) and dissolved in DMSO. Coelenterazine-h was obtained from Promega (Leiden, The Netherlands) and dissolved in methanol.

Primary screen setup

The Spectrum library of 2320 compounds with a wide range of reported biological activities and structural diversity (MicroSource Discovery Systems) was screened for inhibitors of 2,4-D-induced Ca^{2+} signaling. The individual compounds and controls were added to 100 µL YFP-apoaequorin-expressing BY-2 cells in white 96-well plates, with a final concentration of 50 µM per well. Negative (0.5% DMSO) and positive (10 mM $GdCl_3$) controls were added to both outer columns of each multiwell plate. After a 30-minute incubation period in the dark to reduce background signals, 100 µL 2,4-D (final concentration 500 µM) was added to each well with a liquid handling robot (Tecan Freedom EVO200 with 96-channel head) and immediately transferred to the luminescence imaging system (NightSHADE LB 985 *in vivo* Plant Imaging System, Berthold Technologies) to ensure capturing the peak signal in each well. The induced luminescent signal was measured for 30 cycles with a 10-second exposure time per cycle. The maximum signal in each well was calculated and normalized to the average of the negative control of the corresponding multiwell plate.

Luminescence measurements of Ca^{2+} responses in BY-2 cells during confirmation screen and follow-up experiments

Five days after subculturing, YFP-apoAEQ-expressing BY-2 cells were collected by centrifugation, washed, and resuspended in fresh BY-2 medium. Aequorin was reconstituted in the BY-2 cells by adding 2.5 µM of coelenterazine-h (Promega, Leiden, The Netherlands)

for 3 hours under agitation in the dark. Afterwards, 100 µL of reconstituted BY-2 cells was added to each well of a white 96-well plate (PerkinElmer), and the cells were preincubated with the hits identified in the primary screen for 30 minutes to 1 hour in the dark. For measuring elicitor-induced Ca^{2+} responses per well, 100 µL elicitor solution was added to the cells, after which the aequorin-induced light emission was measured every 1.5 seconds for 200 seconds (every 2 seconds for 240 seconds during the confirmation screen) with a luminescence plate reader (all measurements were done in a LUMIstar Galaxy, BMG LABTECH, unless mentioned otherwise). Immediately after this measurement, the remaining reconstituted aequorin was discharged by the addition of 50 µL of discharge solution (0.1 M $CaCl_2$ and 20% ethanol (v/v)), and luminescence was measured every 1.5 seconds for an additional 100 seconds (every 2 seconds for 160 seconds during the confirmation screen). The bioluminescence signal of our transgenic BY-2 cell lines could not be converted to absolute $[Ca^{2+}]_{cyt}$ values because the total luminescent signal after aequorin discharge could not be completely detected *in situ* due to saturation of the plate reader detector. Therefore, all treatments were always evaluated relative to controls within each corresponding multiwell plate. This normalization also accounted for day-to-day variation in amplitude and shape of the Ca^{2+} signals.

Luminescence measurements of Ca^{2+} responses in Arabidopsis seedlings

Gas-sterilized seeds were grown on plates containing half-strength Murashige and Skoog (MS) medium for 3 days until germination. Freshly germinated seedlings were transferred individually to wells of sterile, white, 96-well microplates (PerkinElmer) containing 130 µL of medium composed of ½ MS salts (2.2 g/l), 0.5 g/l MES, 1% sucrose, and 0.08% phyto agar. This low phyto agar concentration provided modest support for the growing seedlings while still allowing rapid mixing of injected pretreatment compounds and elicitor solutions. The transparent lids of the 96-well plates were sealed with Parafilm to prevent medium

evaporation. The seedlings were grown in the plates for 2 to 3 days in a growth chamber under continuous light conditions at 21°C. The evening before measurement, 130 µL of water containing 2.5 µM coelenterazine-h (Ctz-h; Promega, Leiden, The Netherlands) was added to each well to allow overnight reconstitution of apoaequorin into functional aequorin. During this incubation, the plate was covered in aluminum foil to prevent light-induced degradation of Ctz-h. The following day, 130 µL of the medium was removed and replaced with 130 µL of a solution containing 2x the final concentrations of the compounds in water. After a 1-hour preincubation period, 130 µL medium was removed just before the luminescence measurements, to allow the addition of elicitor solutions.

The seedling-containing 96-well plates were analyzed in a luminescence plate reader (LUMIstar Galaxy, BMG LABTECH). Luminescence was first measured every 0.3 seconds for 6 seconds to establish a baseline reading, after which 100 µL of a 2x elicitor solution was automatically added and luminescence was further measured every 0.3 seconds for 54 seconds. Subsequently, the plate was removed from the plate reader and 100 µL of solution was removed from each well. The plate was then placed into the plate reader again and luminescence was measured every 0.3 seconds for 6 seconds to establish a baseline signal. Subsequently, 100 µL of discharge solution (2 M $CaCl_2$ and 50% ethanol) was automatically added and luminescence was further measured every 0.3 seconds for 54 seconds in order to determine the remaining aequorin in the seedlings.

Quantification of Ca^{2+} response data in transgenic YFP-apoaequorin-expressing *Arabidopsis thaliana* seedlings

Raw light data measured by the LUMIstar Galaxy plate reader were converted to calcium concentration by applying the empirically determined formula pCa = 0.332588(-logk) + 5.5593 (Knight et al., 1996). The rate constant k in this formula equals the elicitor-induced

luminescence counts per second divided by the total remaining counts. The total remaining counts were determined after adding discharge solution (2 M $CaCl_2$ + 50% ethanol).

Phenotyping

Wild-type gas-sterilized *Arabidopsis thaliana* seeds were plated on ½ MS medium supplemented with the appropriate compounds and/or hormones (3 rows/plate, 0.5 cm between seeds). For the primary root length experiments, the plated seeds were first stratified for 3 days in the dark at 4°C and subsequently transferred to a growth chamber under continuous light conditions at 21°C. After 7 days of growth, the plates were scanned and the primary root lengths of the seedlings were measured with ImageJ. For each treatment 10-61 individual roots were counted.

Late endosomal marker localization

Three- to four-day-old seedlings from the endomembrane marker lines (2xFYVE-YFP, Ara7-mRFP, and VAMP727-YFP) were pretreated with control medium or 50 µM bepridil for 5 hours. The control medium (CaPLUS) consists of the following components dissolved in MilliQ (for 0.5 liters): 25 mL MS basal salt micronutrient solution, 5 g sucrose, 0.05 g myoinositol, 0.25 g MES, 0.413 g NH_4NO_3, 0.045 g $MgSO_4$, 0.475 g KNO_3, 0.043 g $H_2KO_4P^-$, and 0.083 g $CaCl_2$, with pH set to 5.7.

For imaging of the endomembrane markers, the confocal laser scanning microscopes Leica SP2 (Leica Microsystems) and Zeiss 710 (Zeiss) were used. Fluorescence emission of mRFP (ex 561 nm/em 570-630 nm) and YFP (ex 514 nm/em 520-565 nm) was detected using a 63x water objective (NA 1.2, digital zoom 1,2x). Images were analyzed using Fiji (Schindelin et al., 2012).

R-GECO1 visualization

Seedlings from the R-GECO1 line were pretreated for 30 minutes with 50 µM bepridil or 0.1% DMSO and mounted in a specialized imaging chamber as previously described (Himschoot et al., 2018). The imaging chamber was mounted on the stage of an Ultra View Vox spinning disc microscope (PerkinElmer) and 250 nM IAA was added to elicit a Ca^{2+} response in the samples. R-GECO1 fluorescence intensity was monitored for 8 minutes after elicitor addition and processed as previously described (Himschoot et al., 2018). Per treatment, 3-4 individual measurements were performed.

DR5rev::VENUS-N7 visualization

DR5rev::VENUS-N7 seedlings were grown for 5 days on ½ MS plates containing the appropriate compounds or 0.1% DMSO. For each treatment, 5 seedlings were stained with freshly prepared PI solution (15 µM in distilled water) for 2 minutes, rinsed twice in water, and subsequently spread on a glass microscope slide. Fluorescence emission of DR5rev::VENUS-N7 (ex 514 nm/em 535-590 nm) and PI (ex 514 nm/em 570-630 nm) was visualized and imaged using a Leica SP2 confocal microscope (Leica Microsystems).

Analysis of vacuolar morphology

Analysis of vacuolar morphology was carried out on 6-day-old seedlings of a tonoplast marker line (pUBQ10::VAMP711-YFP) that were grown on solid ½ MS medium. The samples were pretreated for 5 hours with 50 µM bepridil or solvent control (DMSO). Subsequently, the seedlings were transferred to plates containing either DMSO, 50 µM bepridil, 250 nM IAA, or bepridil and IAA (50 µM and 250 nM, respectively). Afterwards, seedlings were grown for another 3 hours prior to image acquisition. Roots were mounted in PI solution (0.02 mg/mL) to counterstain cell walls and report viability. YFP was excited at 514 nm (fluorescence

emission: 525 nm - 555 nm) and PI at 561 nm (fluorescence emission: 644 - 753 nm) using a Leica TCS SP5 confocal laser scanning microscope equipped with a Leica HCX PL APO CS 63 × 1.20 water-immersion objective. Confocal images were analyzed using ImageJ. To calculate the vacuolar morphology index, the longest and widest distance of the biggest luminal structure was measured and multiplied (Lofke et al., 2015). The atrichoblast cells were quantified before the onset of elongation (late meristematic). To depict this region, the first cell being twice as long as wide was considered as the onset of elongation. Starting from this cell, the next cell towards the meristem was excluded (as it usually shows either partial elongation and/or already substantial vacuolar expansion), and vacuoles of the subsequent 4 cells were quantified as described previously (Dünser et al., 2017).

BY-2 viability assay

Five-day-old BY-2 cells were treated with H_2O, 1% DMSO, 500 µM 2,4-D, or a combination of 1% DMSO and 500 µM 2,4-D. After 1 hour of treatment, the cells were stained with freshly prepared FDA-PI staining solution (15 µM FDA and 15 µM PI in BY-2 medium) for 5 minutes in the dark. Afterwards, the cells were washed with fresh medium and 100 µL of cells was spread on a glass microscope slide per treatment. For each treatment, approximately 100 cells were counted using an Ultra View Vox spinning disc microscope (PerkinElmer) and classified as alive or dead based on their individual uptake of FDA and PI. For each treatment, 2-4 such individual measurements were performed.

ATP content determination

Wild-type tobacco BY-2 cell cultures were used and maintained as described earlier. Five days after subculturing, the BY-2 cell suspension was diluted 5 times in modified LS medium and preconditioned in the dark for 1 hour on a shaker before use. The cells were

subsequently distributed in white 96-well plates (95 µL/well) and 5 µL of the appropriate compounds (DMSO, cloxyquin (50 and 20 µM final concentration), niclosamide (50 and 20 µM final concentration), (+)-usnic acid (50 and 20 µM final concentration), and CCCP (20 µM final concentration)) was added with a Freedom EVO robot (Tecan). All compounds were dissolved in DMSO with the final DMSO concentration for each treatment being 0.66%. There were 8 repeats per treatment. The ATP levels were detected by adding 80 µL of the ATPlite 1step Luminescence Assay System (PerkinElmer) after incubation of the cells in the presence of the compounds for the indicated time. Luminescence was measured with an EnVision 2104 Multilabel Reader (PerkinElmer).

Accession Numbers

Sequence data from this article can be found in the GenBank/EMBL data libraries under accession numbers E14214.1 (apoaequorin), JN258411.1 (R-GECO1), NM_115290.5 (VAMP727-At3g54300) and NM_119367.3 (VAMP711- AT4G32150).

Supplemental Material

Supplemental Fig. S1. DMSO and 2,4-D have no significant impact on BY-2 cell viability.

Supplemental Fig. S2. Overview of chemical structures.

Supplemental Fig. S3. Higher magnification of root phenotypes of fenamate-treated plants.

Supplemental Fig. S4. Diphenylamine, aniline, and anthranilic acid make roots resistant to 2,4-D.

Supplemental Fig. S5. Bepridil has a profound impact on endomembrane trafficking.

Supplemental Fig. S6. Bepridil has a profound impact on vacuolar morphology.

Supplemental Fig. S7. The protonophores ES9 and CCCP alter sucrose-induced Ca^{2+} signals.

Supplemental Fig. S8. Imidazoles are not robust inhibitors of 2,4-D induced Ca^{2+}.

Supplemental References. References for Supplemental Table S1.

Supplemental Table S1. List of confirmed hit compounds (excel file).

Supplemental Video S1. B**epridil** inhibits the **IAA-induced Ca^{2+} response in** Arabidopsis **roots expressing R-GECO1** (.avi file)

Tables

Table 1. Thirteen compounds selected for further validation experiments

Name	Reported Bioactivities	Reference
Artemether	antimalarial agent, HMGCoA inhibitor	Korade et al., 2016
Bepridil hydrochloride	calcium-blocking agent, antiarrhythmic, antihypertensive, calmodulin antagonist	Narahara et al., 1992
Clotrimazole	antifungal, antibacterial, sterol biosynthesis inhibitor	Qiu et al., 2017
Cloxyquin	antibacterial, antifungal	Hongmanee et al., 2007
Dicyclomine hydrochloride	anticholinergic	Ali et al., 2018
Flufenamic acid	anti-inflammatory, analgesic, antipyretic	Habjan and Vandenberg, 2009
Niclosamide	anthelmintic, teniacide	Monin et al., 2016
Niflumic acid	analgesic, anti-inflammatory	Hogg et al., 1994
Oxiconazole nitrate	antifungal, sterol biosynthesis inhibitor	Jegasothy and Pakes, 1991
Tannic acid	nonspecific enzyme/receptor blocker	Isenburg et al., 2005
Tolfenamic acid	anti-inflammatory, analgesia	Pentikainen et al., 1981
Triclosan	anti-infective, antibacterial, antifungal	Heath et al., 1999
(+)-Usnic acid	antibacterial	Latkowska et al., 2006

Acknowledgments

We thank Dr. Simon Stael for critical reading of the manuscript.

Figure Legends

Fig. 1. Fourteen elicitors induce a distinct Ca^{2+} signal in aequorin-expressing BY-2 cells. (A) Schematic representation of aequorin complex formation and bioluminescent reaction. A functional aequorin complex is formed upon binding of apoaequorin with its substrate coelenterazine (CTZ) in the presence of O_2. The binding of three Ca^{2+} ions leads to the conversion of CTZ into coelenteramide (CTA) and CO_2, upon which blue light (λ = 469 nm) is emitted. **(B-O)** Ca^{2+} response of YFP-apoaequorin-expressing BY-2 cells treated with various potential elicitors: **(B)** 0.5 M D-glucose, **(C)** 0.5 M sucrose, **(D)** 0.5 M D-mannitol, **(E)** 0.5 M D-sorbitol, **(F)** 0.3 M NaCl, **(G)** 167 µM and 500 µM ATP, **(H)** 167 µM and 500 µM IAA, **(I)** 20 µM and 500 µM NAA, **(J)** 167 µM and 500 µM 2,4-D, **(K)** 5 mM salicylic acid (SA), **(L)** 167 µM and 500 µM gibberellin (GA_3), **(M)** 167 µM and 500 µM 6-benzylaminopurine (6-BAP), **(N)** 125 nM flg22, and **(O)** 5 mM H_2O_2. The data represent average luminescence values of 3 individual measurements in the same multiwell plate. Error bars represent ± SEM.

Fig. 2. Schematic representation of primary screen for Ca^{2+} signaling inhibitors. (A-B) Multiwell setup for screening inhibitors of auxin-induced Ca^{2+} responses via YFP-apoaequorin-expressing BY-2 cells. Based on the means and standard deviations of both the positive (10 mM $GdCl_3$, purple) and negative (0.5% DMSO, cyan) controls of a test run, a Z' score of 0.54 could be calculated **(A)**, supporting the robustness of the assay. Using this setup, the Spectrum library of 2320 compounds was screened for inhibitors of 2,4-D-induced Ca^{2+} signaling **(B)**. The outer columns contained positive (10 mM $GdCl_3$, purple) and negative (0.5% DMSO, cyan) controls, with the assay compounds in the 10 inner columns (50 µM; white). Addition of auxin induced a rapid luminescence-based signal that was detected with the NightSHADE luminescence imaging system. From this library, 80 hit compounds were retained that caused a maximum signal less than 55% of that of the DMSO-treated control cells. **(C)** Confirmation screen of the 80 hit compounds in a multiwell

plate reader. After 240 seconds, 50 µL discharge solution (0.1 M $CaCl_2$ and 20% ethanol) was added and luminescence was measured for the remaining 160 seconds. Based on their Ca^{2+} response and burst patterns, the tested compounds could be further categorized into 4 groups: confirmed (green), semiconfirmed (yellow), cytotoxic (blue), and false-positive (red) compounds. **(D)** Maximum 2,4-D-induced Ca^{2+} response signal of YFP-apoaequorin-expressing BY-2 cells pretreated with 50 µM of 13 selected hit compounds. The data represent average maximum luminescence values of 4-8 individual measurements in comparison to the average of 4-8 DMSO controls in the same multiwell plate. Error bars represent ± SEM. Bars are color-coded based on the underlying Ca^{2+} response and burst patterns. Student's t-test p-values: *p < 0.05, **p < 0.01, and ***p < 0.001. Bepr., bepridil; FFA, flufenamic acid; NFA, niflumic acid; TFA, tolfenamic acid; Clot., clotrimazole; Ox. Nit., oxiconazole nitrate; Art., artemether; Nicl., niclosamide; U.A., (+)-usnic acid; Clox., cloxyquin; Dic. Hyd., dicyclomine hydrochloride; T.A., tannic acid; Tricl., triclosan.

Fig. 3. Fenamates alter the shape of auxin-induced Ca^{2+}. (A-C) 2,4-D-induced Ca^{2+} response of YFP-apoaequorin-expressing BY-2 cells treated with 50 µM FFA **(A)**, NFA **(B)**, or TFA **(C)**. Discharge solution was added after 200 seconds. The data represent average luminescence values of 4-8 individual measurements (solid lines) in comparison to the average of 4-8 DMSO controls (dotted lines) in the same multiwell plate. Error bars represent ± SEM. **(D)** Phenotype of WT Col-0 seedlings grown for 7 days in presence of 0.1% DMSO or 20 µM FFA, NFA, or TFA. **(E)** Vertical Growth Index (VGI) values for the roots from (D). For each treatment, 42 to 47 roots were measured. Student's t-test p-values: ***p < 0.001. **(F-H)** Confocal microscopy images of 5-day-old DR5rev::VENUS-N7 seedlings grown on 0.1% DMSO **(F)**, 20 µM FFA **(G)**, and 20 µM TFA **(H)**. Green: DR5rev::VENUS-N7 signal; red: propidium iodide staining.

Fig. 4. Functional and structural fenamate analogs do not alter the shape of auxin-induced Ca^{2+}. (A) Overview of a small-scale SAR analysis of the fenamates. Based on known and observed functions and structures of the hit fenamates, a set of functional and structural analogs was investigated. **(B-C)** 2,4-D-induced Ca^{2+} response of YFP-apoaequorin-expressing BY-2 cells treated with 50 µM of the auxin transport inhibitors BUM **(B)** and NPA **(C)**. Discharge solution was added after 200 seconds. The data represent average luminescence values of 4 individual measurements (solid lines) in comparison to the average of 4 DMSO controls (dotted lines) in the same multiwell plate. Error bars represent ± SEM. **(D-E)** 2,4-D-induced Ca^{2+} response of YFP-apoaequorin-expressing BY-2 cells treated with 50 µM of the NSAIDs ibuprofen **(D)** and oxaprozin **(E)** (note: measurements were done with a new plate reader (GloMax Navigator - Promega) because the old one was defective). The data represent average luminescence values of 8 individual measurements (solid lines) in comparison to the average of 8 DMSO controls (dotted lines) in the same multiwell plate. Error bars represent ± SEM. **(F-L)** 2,4-D-induced Ca^{2+} response of YFP-apoaequorin-expressing BY-2 cells treated with 50 µM of 2 anion channel inhibitors (9-ACA and NPPB; **F-G**) and various compounds structurally similar to fenamates **(H-L)**. Discharge solution was added after 200 seconds. The data represent average luminescence values of 4 individual measurements (solid lines) in comparison to the average of 4 DMSO controls (dotted lines) in the same multiwell plate. Error bars represent ± SEM. BUM, 2-[4-(diethylamino)-2-hydroxybenzoyl]benzoic acid; NPA, 1-N-naphtylphtalamic acid; 9-ACA, 9-anthracenecarboxylic acid; NPPB, 5-nitro-2-(3-phenylpropylamino) benzoic acid; α-ph.-o-tol. acid, α-phenyl-o-toluic acid; A.U., arbitrary units.

Fig. 5. Protonophores impair the 2,4-D-induced Ca^{2+} response and render roots insensitive to 2,4-D. (A-C) 2,4-D-induced Ca^{2+} response of YFP-apoaequorin-expressing BY-2 cells treated with 50 µM niclosamide **(A)**, (+)-usnic acid **(B)**, or cloxyquin **(C)**. Discharge solution was added after 200 seconds. The data represent average luminescence values of 4

individual measurements (solid lines) in comparison to the average of 4 DMSO controls (dotted lines) in the same multiwell plate. Error bars represent ± SEM. **(D)** Maximum 2,4-D-induced luminescence in YFP-apoaequorin-expressing BY-2 cells treated with 50 µM of the hit protonophores niclosamide and (+)-usnic acid, the ionophore valinomycin, or the non-hit protonophores tyrphostin A23, CCCP, and ES9. Four individual measurements were performed for each treatment and compared to the average of 8 DMSO controls in the same multiwell plate. Error bars represent ± SEM. Student's t-test p-values: **p < 0.01 and ***p < 0.001. **(E)** ATP measurements of BY-2 cells pretreated with 0.5% DMSO (white), 20 µM CCCP (black), or 20 µM or 50 µM cloxyquin (dots), niclosamide (diagonal stripes), or (+)-usnic acid (horizontal stripes). ATP was measured 2, 10, 30, and 60 minutes after compound treatment. Error bars represent ± SEM. Student's t-test p-values: *p < 0.05, **p < 0.01, and ***p < 0.001. **(F)** Average primary root length of WT Col-0 seedlings grown for 7 days on ½ MS medium in presence of 0.1% DMSO or 20 µM niclosamide, cloxyquin, or (+)-usnic acid (grey bars) and supplemented with 100 nM 2,4-D (red bars) or 20 µM ACC (blue bars). Root lengths represent average of 12-21 roots. Error bars represent ± SEM. Student's t-test p-values: *p < 0.05, **p < 0.01, and ***p < 0.001. **(G-J)** Confocal microscopy images of 5-day-old DR5rev::VENUS-N7 seedlings grown on 0.1% DMSO **(G)**, 20 µM niclosamide **(H)**, 20 µM cloxyquin **(I)**, or 20 µM (+)-usnic acid **(J)**. Green: DR5rev::VENUS-N7 signal; red: propidium iodide staining. The image in **(G)** is identical to Fig. 3F.

Fig. 6. Bepridil is a potent inhibitor of auxin-induced Ca^{2+} signaling. (A) 2,4-D-induced Ca^{2+} response of YFP-apoaequorin-expressing BY-2 cells treated with 50 µM bepridil. Discharge solution was added after 200 seconds. The data represent average luminescence values of 4 individual measurements (solid lines) in comparison to the average of 4 DMSO controls (dotted lines) in the same multiwell plate. Error bars represent ± SEM. **(B)** Fluorescent intensity in R-GECO1-expressing Arabidopsis seedlings after IAA treatment. Seedlings were pretreated for 30 minutes with 50 µM bepridil (solid lines) or 0.1% DMSO

(dotted lines). IAA (250 nM) was added at time point 0, and R-GECO1 fluorescence intensity was monitored for 8 minutes. The data represent average fluorescence values of 4 individual measurements in comparison to the average of 3 DMSO controls. Error bars represent ± SEM. **(C)** Snapshot of the peak Ca^{2+} signal elicited in R-GECO1 seedlings by 250 nM IAA after a 30-minute pretreatment with 0.1% DMSO (left) or 50 µM bepridil (right). The snapshots were taken from Supplemental Video S1 30 seconds after IAA addition. **(D)** Average primary root length of WT Col-0 seedlings grown for 7 days on ½ MS medium in presence of 0.1% DMSO or 10 µM, 20 µM, or 50 µM bepridil. Root lengths represent the average of 54-60 roots. Error bars represent ± SEM. Student's t-test p-value: ***$p < 0.001$. **(E-F)** Confocal microscopy images of 5-day-old DR5rev::VENUS-N7 seedlings grown on 0.1% DMSO **(E)** and 20 µM bepridil **(F)**. Green: DR5rev::VENUS-N7 signal; red: propidium iodide staining. **(G)** Average primary root length of WT Arabidopsis seedlings grown for 7 days on ½ MS medium in presence of 20 µM bepridil or 0.1% DMSO (grey) and supplemented with 100 nM 2,4-D (red), 20 µM ACC (blue), 150 nM NAA (yellow), or 250 nM NAA (green). Root lengths represent the average of 51-61 roots. Error bars represent ± SEM. Student's t-test p-values in comparison to DMSO: **$p < 0.01$ and ***$p < 0.001$. **(H-I)** The effect of bepridil on vacuolar morphology. Six-day-old pUBQ10::VAMP711-YFP seedlings were pretreated with 50 µM bepridil or solvent control for 5 h, followed by 3-h treatments with (DMSO), 250 nM IAA (IAA), 50 µM bepridil (Bepr), or 50 µM bepridil and 250 nM IAA (Bepr + IAA). Tonoplast-localized VAMP711-YFP (orange) as vacuolar marker and propidium iodide stain (green) for decorating the cell wall were used for confocal imaging of atrichoblast cells **(H)**. The quantification of the vacuolar morphology index was performed with 4 vacuoles of late meristematic atrichoblasts per root, with 10-14 roots used for each treatment **(I)**. Statistical analysis was performed using one-way ANOVA (Kruskal-Wallis test) followed by Dunn´s multiple comparison test, b: $p < 0.05$, c: $p < 0.001$.

Fig. 7. Sucrose-induced Ca^{2+} signals are highly sensitive to fenamates, protonophores, and imidazoles. (A-H) Sucrose-induced Ca^{2+} responses of YFP-apoaequorin-expressing Arabidopsis seedlings treated with fenamates **(A-C)**, protonophores **(D-E)**, imidazoles **(F-G)**, or bepridil **(H)**. The data represent average luminescence values of 4 individual measurements (solid lines) in comparison to the average of 4 DMSO controls (dotted lines) in the same multiwell plate. Error bars represent ± SEM. FFA, flufenamic acid; NFA, niflumic acid; TFA, tolfenamic acid; Nicl., niclosamide; U.A., (+)-usnic acid; Clot., clotrimazole; Ox. Nit., oxiconazole nitrate; Bepr., bepridil.

References

Ali A, Jadhav A, Jangid P, Patil R, Shelar A, Karuppayil SM (2018) The human muscarinic acetylcholine receptor antagonist, Dicyclomine targets signal transduction genes and inhibits the virulence factors in the human pathogen, Candida albicans. J Antibiot (Tokyo) **71:** 456-466

Ane JM, Kiss GB, Riely BK, Penmetsa RV, Oldroyd GE, Ayax C, Levy J, Debelle F, Baek JM, Kalo P, Rosenberg C, Roe BA, Long SR, Denarie J, Cook DR (2004) Medicago truncatula DMI1 required for bacterial and fungal symbioses in legumes. Science **303:** 1364-1367

Barbez E, Dünser K, Gaidora A, Lendl T, Busch W (2017) Auxin steers root cell expansion via apoplastic pH regulation in Arabidopsis thaliana. Proc Natl Acad Sci U S A **114:** E4884-E4893

Behera S, Xu Z, Luoni L, Bonza MC, Doccula FG, De Michelis MI, Morris RJ, Schwarzlander M, Costa A (2018) Cellular Ca(2+) Signals Generate Defined pH Signatures in Plants. The Plant cell **30:** 2704-2719

Benjamins R, Ampudia CSG, Hooykaas PJJ, Offringa R (2003) PINOID-mediated signaling involves calcium-binding proteins. Plant Physiology **132:** 1623-1630

Chaiwanon J, Wang W, Zhu JY, Oh E, Wang ZY (2016) Information Integration and Communication in Plant Growth Regulation. Cell **164:** 1257-1268

Charpentier M, Bredemeier R, Wanner G, Takeda N, Schleiff E, Parniske M (2008) Lotus japonicus CASTOR and POLLUX are ion channels essential for perinuclear calcium spiking in legume root endosymbiosis. Plant Cell **20:** 3467-3479

Charpentier M, Sun J, Vaz Martins T, Radhakrishnan GV, Findlay K, Soumpourou E, Thouin J, Very AA, Sanders D, Morris RJ, Oldroyd GE (2016) Nuclear-localized cyclic nucleotide-gated channels mediate symbiotic calcium oscillations. Science **352:** 1102-1105

Clough SJ, Bent AF (1998) Floral dip: a simplified method for Agrobacterium-mediated transformation of Arabidopsis thaliana. The Plant journal : for cell and molecular biology **16:** 735-743

De Vriese K, Costa A, Beeckman T, Vanneste S (2018) Pharmacological Strategies for Manipulating Plant Ca(2+) Signalling. Int J Mol Sci **19**

Dejonghe W, Kuenen S, Mylle E, Vasileva M, Keech O, Viotti C, Swerts J, Fendrych M, Ortiz-Morea FA, Mishev K, Delang S, Scholl S, Zarza X, Heilmann M, Kourelis J, Kasprowicz J, Nguyen le SL, Drozdzecki A, Van Houtte I, Szatmari AM, Majda M, Baisa G, Bednarek SY, Robert S, Audenaert D, Testerink C, Munnik T, Van Damme D, Heilmann I, Schumacher K, Winne J, Friml J, Verstreken P, Russinova E (2016) Mitochondrial uncouplers inhibit clathrin-mediated endocytosis largely through cytoplasmic acidification. Nat Commun **7:** 11710

Dela Fuente RK, Leopold AC (1973) A role for calcium in auxin transport. Plant Physiol **51:** 845-847

Diatloff E, Roberts M, Sanders D, Roberts SK (2004) Characterization of anion channels in the plasma membrane of Arabidopsis epidermal root cells and the identification of a citrate-permeable channel induced by phosphate starvation. Plant Physiol **136:** 4136-4149

Dindas J, Scherzer S, Roelfsema MRG, von Meyer K, Muller HM, Al-Rasheid KAS, Palme K, Dietrich P, Becker D, Bennett MJ, Hedrich R (2018) AUX1-mediated root hair auxin influx governs SCF(TIR1/AFB)-type Ca(2+) signaling. Nat Commun **9:** 1174

Dünser K, Gupta S, Ringli C, Kleine-Vehn J (2017) LRX- and FER-dependent extracellular sensing coordinates vacuolar size for cytosol homeostasis. bioRxiv. Preprint, posted December 8, 2017.

Ebine K, Okatani Y, Uemura T, Goh T, Shoda K, Niihama M, Morita MT, Spitzer C, Otegui MS, Nakano A, Ueda T (2008) A SNARE complex unique to seed plants is required for protein storage vacuole biogenesis and seed development of Arabidopsis thaliana. Plant Cell **20:** 3006-3021

Edel KH, Marchadier E, Brownlee C, Kudla J, Hetherington AM (2017) The Evolution of Calcium-Based Signalling in Plants. Current biology : CB **27:** R667-R679

Fendrych M, Akhmanova M, Merrin J, Glanc M, Hagihara S, Takahashi K, Uchida N, Torii KU, Friml J (2018) Rapid and reversible root growth inhibition by TIR1 auxin signalling. Nat Plants **4:** 453-459

Forde BG, Roberts MR (2014) Glutamate receptor-like channels in plants: a role as amino acid sensors in plant defence? F1000prime reports **6:** 37

Furuichi T, Mori IC, Takahashi K, Muto S (2001) Sugar-induced increase in cytosolic Ca(2+) in Arabidopsis thaliana whole plants. Plant Cell Physiol **42:** 1149-1155

Gao D, Knight MR, Trewavas AJ, Sattelmacher B, Plieth C (2004) Self-reporting Arabidopsis expressing pH and [Ca2+] indicators unveil ion dynamics in the cytoplasm and in the apoplast under abiotic stress. Plant physiology **134:** 898-908

Geldner N, Denervaud-Tendon V, Hyman DL, Mayer U, Stierhof YD, Chory J (2009) Rapid, combinatorial analysis of membrane compartments in intact plants with a multicolor marker set. Plant J **59:** 169-178

Gilliham M, Tester M (2005) The regulation of anion loading to the maize root xylem. Plant Physiol **137:** 819-828

Graham GG (2016) Fenamates. . Parnham M. (eds) Compendium of Inflammatory Diseases.

Habjan S, Vandenberg RJ (2009) Modulation of glutamate and glycine transporters by niflumic, flufenamic and mefenamic acids. Neurochem Res **34:** 1738-1747

Heath RJ, Rubin JR, Holland DR, Zhang E, Snow ME, Rock CO (1999) Mechanism of triclosan inhibition of bacterial fatty acid synthesis. J Biol Chem **274:** 11110-11114

Heisler MG, Ohno C, Das P, Sieber P, Reddy GV, Long JA, Meyerowitz EM (2005) Patterns of auxin transport and gene expression during primordium development revealed by live imaging of the Arabidopsis inflorescence meristem. Curr Biol **15:** 1899-1911

Herrmann A, Felle HH (1995) Tip Growth in Root Hair-Cells of Sinapis-Alba L - Significance of Internal and External Ca2+ and Ph. New Phytologist **129:** 523-533

Himschoot E, Krebs M, Costa A, Beeckman T, Vanneste S (2018) Calcium Ion Dynamics in Roots: Imaging and Analysis. Methods Mol Biol **1761:** 115-130

Hogg RC, Wang Q, Large WA (1994) Action of niflumic acid on evoked and spontaneous calcium-activated chloride and potassium currents in smooth muscle cells from rabbit portal vein. Br J Pharmacol **112:** 977-984

Hongmanee P, Rukseree K, Buabut B, Somsri B, Palittapongarnpim P (2007) In vitro activities of cloxyquin (5-chloroquinolin-8-ol) against Mycobacterium tuberculosis. Antimicrob Agents Chemother **51:** 1105-1106

Isenburg JC, Simionescu DT, Vyavahare NR (2005) Tannic acid treatment enhances biostability and reduces calcification of glutaraldehyde fixed aortic wall. Biomaterials **26:** 1237-1245

Jegasothy BV, Pakes GE (1991) Oxiconazole nitrate: pharmacology, efficacy, and safety of a new imidazole antifungal agent. Clin Ther **13:** 126-141

Jia T, Gao C, Cui Y, Wang J, Ding Y, Cai Y, Ueda T, Nakano A, Jiang L (2013) ARA7(Q69L) expression in transgenic Arabidopsis cells induces the formation of enlarged multivesicular bodies. J Exp Bot **64:** 2817-2829

Keinath NF, Waadt R, Brugman R, Schroeder JI, Grossmann G, Schumacher K, Krebs M (2015) Live Cell Imaging with R-GECO1 Sheds Light on flg22- and Chitin-Induced Transient [Ca(2+)]cyt Patterns in Arabidopsis. Mol Plant **8:** 1188-1200

Knight H, Trewavas AJ, Knight MR (1996) Cold calcium signaling in Arabidopsis involves two cellular pools and a change in calcium signature after acclimation. Plant Cell **8:** 489-503

Knight MR, Campbell AK, Smith SM, Trewavas AJ (1991) Transgenic plant aequorin reports the effects of touch and cold-shock and elicitors on cytoplasmic calcium. Nature **352:** 524-526

Korade Z, Kim HY, Tallman KA, Liu W, Koczok K, Balogh I, Xu L, Mirnics K, Porter NA (2016) The Effect of Small Molecules on Sterol Homeostasis: Measuring 7-Dehydrocholesterol in Dhcr7-Deficient Neuro2a Cells and Human Fibroblasts. J Med Chem **59:** 1102-1115

Kudla J, Batistic O, Hashimoto K (2010) Calcium signals: the lead currency of plant information processing. Plant Cell **22:** 541-563

Kudla J, Becker D, Grill E, Hedrich R, Hippler M, Kummer U, Parniske M, Romeis T, Schumacher K (2018) Advances and current challenges in calcium signaling. The New phytologist **218:** 414-431

Lanner JT, Georgiou DK, Joshi AD, Hamilton SL (2010) Ryanodine receptors: structure, expression, molecular details, and function in calcium release. Cold Spring Harbor perspectives in biology **2:** a003996

Latkowska E, Lechowski Z, Bialczyk J, Pilarski J (2006) Photosynthesis and water relations in tomato plants cultivated long-term in media containing (+)-usnic acid. J Chem Ecol **32:** 2053-2066

Lavy M, Estelle M (2016) Mechanisms of auxin signaling. Development **143:** 3226-3229

Lipsanen A, Flunkert S, Kuptsova K, Hiltunen M, Windisch M, Hutter-Paier B, Jolkkonen J (2013) Non-selective calcium channel blocker bepridil decreases secondary pathology in mice after photothrombotic cortical lesion. PLoS One **8:** e60235

Liu J, Moore S, Chen C, Lindsey K (2017) Crosstalk Complexities between Auxin, Cytokinin, and Ethylene in Arabidopsis Root Development: From Experiments to Systems Modeling, and Back Again. Molecular plant **10:** 1480-1496

Lofke C, Dunser K, Scheuring D, Kleine-Vehn J (2015) Auxin regulates SNARE-dependent vacuolar morphology restricting cell size. Elife **4**

Ma W, Berkowitz GA (2011) Ca2+ conduction by plant cyclic nucleotide gated channels and associated signaling components in pathogen defense signal transduction cascades. The New phytologist **190:** 566-572

Mehlmer N, Parvin N, Hurst CH, Knight MR, Teige M, Vothknecht UC (2012) A toolset of aequorin expression vectors for in planta studies of subcellular calcium concentrations in Arabidopsis thaliana. J Exp Bot **63:** 1751-1761

Michard E, Simon AA, Tavares B, Wudick MM, Feijo JA (2017) Signaling with Ions: The Keystone for Apical Cell Growth and Morphogenesis in Pollen Tubes. Plant Physiology **173:** 91-111

Monin MB, Krause P, Stelling R, Bocuk D, Niebert S, Klemm F, Pukrop T, Koenig S (2016) The anthelmintic niclosamide inhibits colorectal cancer cell lines via modulation of the canonical and noncanonical Wnt signaling pathway. J Surg Res **203:** 193-205

Monshausen GB, Bibikova TN, Weisenseel MH, Gilroy S (2009) Ca2+ regulates reactive oxygen species production and pH during mechanosensing in Arabidopsis roots. The Plant cell **21:** 2341-2356

Monshausen GB, Messerli MA, Gilroy S (2008) Imaging of the Yellow Cameleon 3.6 indicator reveals that elevations in cytosolic Ca(2+) follow oscillating increases in growth in root hairs of arabidopsis. Plant Physiology **147:** 1690-1698

Murthy SE, Dubin AE, Whitwam T, Jojoa-Cruz S, Cahalan SM, Mousavi SAR, Ward AB, Patapoutian A (2018) OSCA/TMEM63 are an Evolutionarily Conserved Family of Mechanically Activated Ion Channels. eLife **7**

Nagata T, Iizumi S, Satoh K, Ooka H, Kawai J, Carninci P, Hayashizaki Y, Otomo Y, Murakami K, Matsubara K, Kikuchi S (2004) Comparative analysis of plant and animal calcium signal transduction element using plant full-length cDNA data. Molecular biology and evolution **21:** 1855-1870

Narahara KA, Singh BN, Karliner JS, Corday SR, Hossack KF (1992) Bepridil hydrochloride compared with placebo in patients with stable angina pectoris. Am J Cardiol **69:** 37D-42D

Nixon GF, Mignery GA, Somlyo AV (1994) Immunogold localization of inositol 1,4,5-trisphosphate receptors and characterization of ultrastructural features of the sarcoplasmic reticulum in phasic and tonic smooth muscle. Journal of muscle research and cell motility **15:** 682-700

Pentikainen PJ, Neuvonen PJ, Backman C (1981) Human pharmacokinetics of tolfenamic acid, a new anti-inflammatory agent. Eur J Clin Pharmacol **19:** 359-365

Philippar K, Ivashikina N, Ache P, Christian M, Luthen H, Palme K, Hedrich R (2004) Auxin activates KAT1 and KAT2, two K+-channel genes expressed in seedlings of Arabidopsis thaliana. Plant J **37:** 815-827

Qiu W, Ren B, Dai H, Zhang L, Zhang Q, Zhou X, Li Y (2017) Clotrimazole and econazole inhibit Streptococcus mutans biofilm and virulence in vitro. Arch Oral Biol **73:** 113-120

Rigo G, Ayaydin F, Tietz O, Zsigmond L, Kovacs H, Pay A, Salchert K, Darula Z, Medzihradszky KF, Szabados L, Palme K, Koncz C, Cseplo A (2013) Inactivation of plasma membrane-localized CDPK-RELATED KINASE5 decelerates PIN2 exocytosis and root gravitropic response in Arabidopsis. The Plant cell **25:** 1592-1608

Sarajarvi T, Lipsanen A, Makinen P, Peraniemi S, Soininen H, Haapasalo A, Jolkkonen J, Hiltunen M (2012) Bepridil decreases Abeta and calcium levels in the thalamus after middle cerebral artery occlusion in rats. J Cell Mol Med **16:** 2754-2767

Scheuring D, Lofke C, Kruger F, Kittelmann M, Eisa A, Hughes L, Smith RS, Hawes C, Schumacher K, Kleine-Vehn J (2016) Actin-dependent vacuolar occupancy of the cell determines auxin-induced growth repression. Proceedings of the National Academy of Sciences of the United States of America **113:** 452-457

Schindelin J, Arganda-Carreras I, Frise E, Kaynig V, Longair M, Pietzsch T, Preibisch S, Rueden C, Saalfeld S, Schmid B, Tinevez JY, White DJ, Hartenstein V, Eliceiri K, Tomancak P, Cardona A (2012) Fiji: an open-source platform for biological-image analysis. Nat Methods **9:** 676-682

Shih HW, DePew CL, Miller ND, Monshausen GB (2015) The Cyclic Nucleotide-Gated Channel CNGC14 Regulates Root Gravitropism in Arabidopsis thaliana. Curr Biol **25:** 3119-3125

Shimomura O (2005) The discovery of aequorin and green fluorescent protein. Journal of microscopy **217:** 1-15

Shimomura O, Johnson FH, Saiga Y (1962) Extraction, purification and properties of aequorin, a bioluminescent protein from the luminous hydromedusan, Aequorea. J Cell Comp Physiol **59:** 223-239

Stephan AB, Kunz HH, Yang E, Schroeder JI (2016) Rapid hyperosmotic-induced Ca2+ responses in Arabidopsis thaliana exhibit sensory potentiation and involvement of plastidial KEA transporters. Proc Natl Acad Sci U S A **113:** E5242-5249

Swarup R, Friml J, Marchant A, Ljung K, Sandberg G, Palme K, Bennett M (2001) Localization of the auxin permease AUX1 suggests two functionally distinct hormone transport pathways operate in the Arabidopsis root apex. Genes & development **15:** 2648-2653

965 **Thiel G, Weise R** (1999) Auxin augments conductance of K+ inward rectifier in maize coleoptile protoplasts.
966 Planta **208:** 38-45
967 **Thomine S, Zimmerman S, Van Duijn B, Barbier-Brygoo H, Guern J** (1994) Calcium channel antagonists
968 induce direct inhibition of the outward rectifying potassium channel in tobacco protoplasts. FEBS Lett
969 **340:** 45-50
970 **Tuteja N, Mahajan S** (2007) Calcium signaling network in plants: an overview. Plant Signal Behav **2:** 79-85
971 **Vanneste S, Friml J** (2009) Auxin: a trigger for change in plant development. Cell **136:** 1005-1016
972 **Vermeer JE, van Leeuwen W, Tobena-Santamaria R, Laxalt AM, Jones DR, Divecha N, Gadella TW, Jr.,**
973 **Munnik T** (2006) Visualization of PtdIns3P dynamics in living plant cells. The Plant journal : for cell and
974 molecular biology **47:** 687-700
975 **Weijers D, Wagner D** (2016) Transcriptional Responses to the Auxin Hormone. Annual review of plant biology
976 **67:** 539-574
977 **Yang Y, Hammes UZ, Taylor CG, Schachtman DP, Nielsen E** (2006) High-affinity auxin transport by the AUX1
978 influx carrier protein. Current biology : CB **16:** 1123-1127
979 **Yatani A, Brown AM, Schwartz A** (1986) Bepridil block of cardiac calcium and sodium channels. J Pharmacol
980 Exp Ther **237:** 9-17
981 **Yuan F, Yang H, Xue Y, Kong D, Ye R, Li C, Zhang J, Theprungsirikul L, Shrift T, Krichilsky B, Johnson**
982 **DM, Swift GB, He Y, Siedow JN, Pei ZM** (2014) OSCA1 mediates osmotic-stress-evoked Ca2+
983 increases vital for osmosensing in Arabidopsis. Nature **514:** 367-371
984 **Zhang J, Vanneste S, Brewer PB, Michniewicz M, Grones P, Kleine-Vehn J, Lofke C, Teichmann T, Bielach**
985 **A, Cannoot B, Hoyerova K, Chen X, Xue HW, Benkova E, Zazimalova E, Friml J** (2011) Inositol
986 trisphosphate-induced Ca2+ signaling modulates auxin transport and PIN polarity. Dev Cell **20:** 855-866
987 **Zhang JH, Chung TD, Oldenburg KR** (1999) A Simple Statistical Parameter for Use in Evaluation and Validation
988 of High Throughput Screening Assays. Journal of biomolecular screening **4:** 67-73
989 **Zhang M, Wang D, Kang Y, Wu JX, Yao F, Pan C, Yan Z, Song C, Chen L** (2018) Structure of the
990 mechanosensitive OSCA channels. Nature structural & molecular biology **25:** 850-858
991 **Zuccotti A, Clementi S, Reinbothe T, Torrente A, Vandael DH, Pirone A** (2011) Structural and functional
992 differences between L-type calcium channels: crucial issues for future selective targeting. Trends in
993 pharmacological sciences **32:** 366-375
994
995

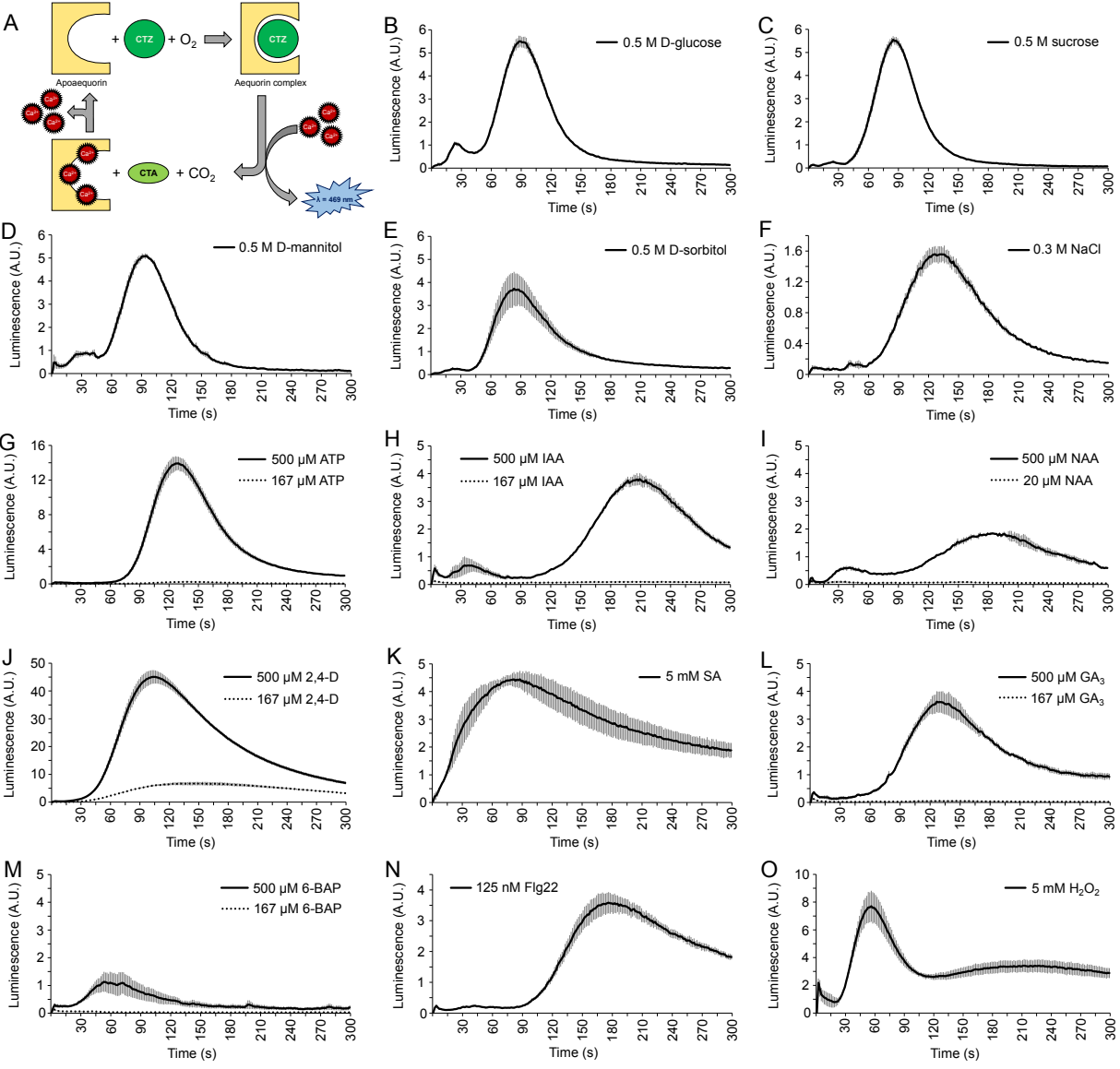

Fig. 1. 14 elicitors induce a distinct Ca^{2+} signal in aequorin-expressing BY-2 cells. (A) Schematic representation of aequorin complex formation and bioluminescent reaction. A functional aequorin complex is formed upon binding of apoaequorin with its substrate coelenterazine (CTZ) in presence of O_2. The binding of three Ca^{2+} ions leads to the conversion of CTZ into coelenteramide (CTA) and CO_2, upon which blue light (λ = 469 nm) is emitted. **(B-O)** Ca^{2+} response of YFP-apoaequorin-expressing BY-2 cells treated with various potential elicitors: **(B)** 0.5 M D-glucose, **(C)** 0.5 M sucrose, **(D)** 0.5 M D-mannitol, **(E)** 0.5 M D-sorbitol, **(F)** 0.3 M NaCl, **(G)** 167 µM and 500 µM ATP, **(H)** 167 µM and 500 µM IAA, **(I)** 20 µM and 500 µM NAA, **(J)** 167 µM and 500 µM 2,4-D, **(K)** 5 mM salicylic acid (SA), **(L)** 167 µM and 500 µM gibberellin (GA_3), **(M)** 167 µM and 500 µM 6-benzylaminopurine (6-BAP), **(N)** 125 nM flg22, **(O)** 5 mM H_2O_2. The data is represented by average luminescence values of 3 individual measurements in the same multi-well plate. Error bars represent ± SEM.

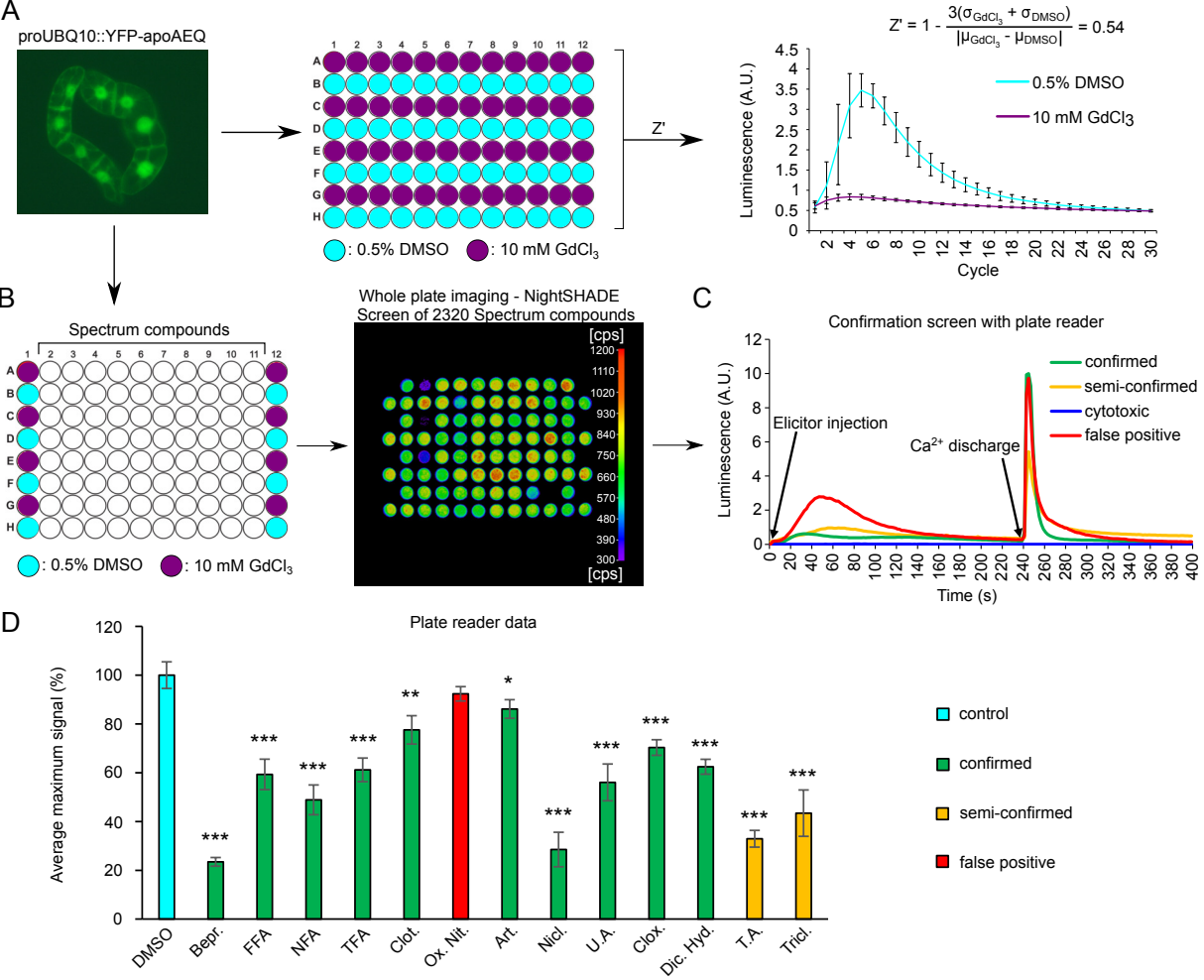

Fig. 2. Schematic representation of primary screen for Ca^{2+} signaling inhibitors. (A-B) Multi-well setup for screening inhibitors of auxin-induced Ca^{2+} responses via YFP-apoaequorin-expressing BY-2 cells. Based on the means and standard deviations of both the positive (10 mM $GdCl_3$, purple) and negative (0.5% DMSO, cyan) controls of a test run, a Z' score of 0.54 could be calculated **(A)**, supporting the robustness of the assay. Using this setup, the Spectrum library of 2320 compounds was screened for inhibitors of 2,4-D-induced Ca^{2+} signaling **(B)**. The outer columns contained positive (10 mM $GdCl_3$, purple) and negative (0.5% DMSO, cyan) controls, with the assay compounds in the 10 inner columns (50 µM; white). Addition of auxin induced a rapid luminescence-based signal that was detected with the NightSHADE luminescence imaging system. From this library, 80 hit compounds were retained that caused a maximum signal less than 55% of that of the DMSO-treated control cells. **(C)** Confirmation screen of the 80 hit compounds in a multi-well plate reader. After 240 seconds, 50 µl discharge solution (0.1 M $CaCl_2$ and 20% ethanol) was added and luminescence was measured for the remaining 160 seconds. Based on their Ca^{2+} response and burst patterns, the tested compounds could be further categorized into 4 groups: confirmed (green), semi-confirmed (yellow), cytotoxic (blue) and false positive (red) compounds, for which example patterns are shown. **(D)** Maximum 2,4-D-induced Ca^{2+} response signal of YFP-apoaequorin-expressing BY-2 cells pre-treated with 50 µM of 13 selected hit compounds. The data is represented by average maximum luminescence values of 4-8 individual measurements in comparison to the average of 4-8 DMSO controls in the same multi-well plate. Error bars represent ± SEM. Bars are color-coded based on the underlying Ca^{2+} response and burst patterns. Student's t-test p-values: *p < 0.05, **p < 0.01, ***p < 0.001. Bepr., bepridil; FFA, flufenamic acid; NFA, niflumic acid; TFA, tolfenamic acid; Clot., clotrimazole; Ox. Nit., oxiconazole nitrate; Art., artemether; Nicl., niclosamide; U.A., (+)-usnic acid; Clox., cloxyquin; Dic. Hyd., dicyclomine hydrochloride; T.A., tannic acid; Tricl., triclosan.

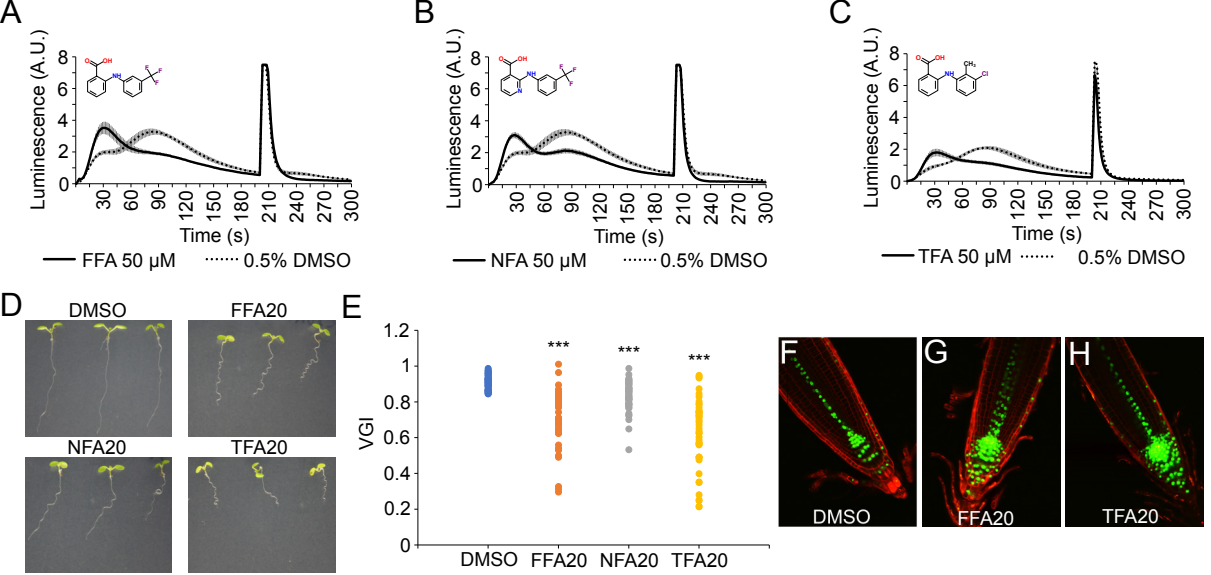

Fig. 3. Fenamates alter the shape of auxin-induced Ca^{2+}. (A-C) 2,4-D-induced Ca^{2+} response of YFP-apoaequorin-expressing BY-2 cells treated with 50 µM FFA **(A)**, NFA **(B)** or TFA **(C)**. Discharge solution was added after 200 seconds. The data is represented by average luminescence values of 4-8 individual measurements (solid lines) in comparison to the average of 4-8 DMSO controls (dotted lines) in the same multi-well plate. Error bars represent ± SEM. **(D)** Phenotype of WT Col-0 seedlings grown for 7 days on ½ MS medium in presence of 0.1% DMSO or 20 µM FFA, NFA or TFA, respectively. **(E)** The Vertical Growth Index (VGI) values for the roots from (D). For each treatment, 42 - 47 roots were measured. Student's *t*-test p-values: ***p < 0.001. **(F-H)** Confocal microscopic images of 5-day-old DR5rev::VENUS-N7 seedlings grown on 0.1% DMSO **(F)**, 20 µM FFA **(G)** and 20 µM TFA **(H)**, respectively. Green: DR5rev::VENUS-N7 signal; Red: propidium iodide staining.

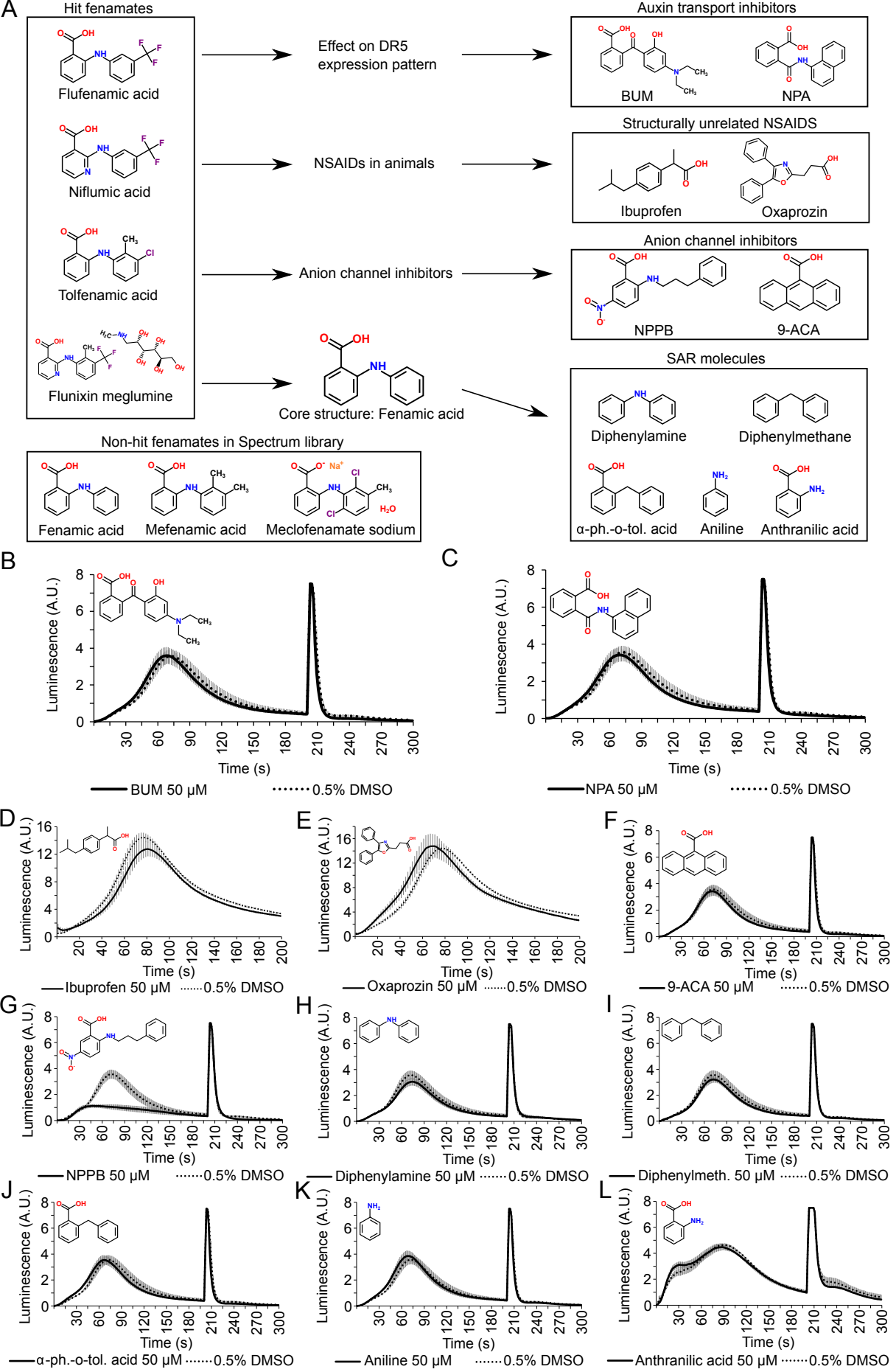

Fig. 4. Functional and structural fenamate analogs do not alter the shape of auxin-induced Ca^{2+}. (A) Overview of a small-scale SAR analysis of the fenamates. Based on known and observed functions and structures of the hit fenamates, a set of functional and structural analogs was investigated. **(B-C)** 2,4-D-induced Ca^{2+} response of YFP-apoaequorin-expressing BY-2 cells treated with 50 µM of the auxin transport inhibitors BUM **(B)** and NPA **(C)**. Discharge solution was added after 200 seconds. The data is represented by average luminescence values of 4 individual measurements (solid lines) in comparison to the average of 4 DMSO controls (dotted lines) in the same multi-well plate. Error bars represent ± SEM. **(D-E)** 2,4-D-induced Ca^{2+} response of YFP-apoaequorin-expressing BY-2 cells treated with 50 µM of the NSAIDs ibuprofen **(D)** and oxaprozin **(E)** (Measurement in GloMax Navigator platereader (Promega)). The data is represented by average luminescence values of 8 individual measurements (solid lines) in comparison to the average of 8 DMSO controls (dotted lines) in the same multi-well plate. Error bars represent ± SEM. **(F-L)** 2,4-D-induced Ca^{2+} response of YFP-apoaequorin-expressing BY-2 cells treated with 50 µM of 2 anion channel inhibitors (9-ACA and NPPB; **F-G**) and various compounds structurally similar to fenamates **(H-L)**. Discharge solution was added after 200 seconds. The data is represented by average luminescence values of 4 individual measurements (solid lines) in comparison to the average of 4 DMSO controls (dotted lines) in the same multi-well plate. Error bars represent ± SEM. BUM, 2-[4-(diethylamino)-2-hydroxybenzoyl]benzoic acid; NPA, 1-N-naphtylphtalamic acid; 9-ACA, 9-anthracenecarboxylic acid; NPPB, 5-nitro-2-(3-phenylpropylamino) benzoic acid; α-ph.-o-tol. acid, α-phenyl-o-toluic acid; A.U., arbitrary units.

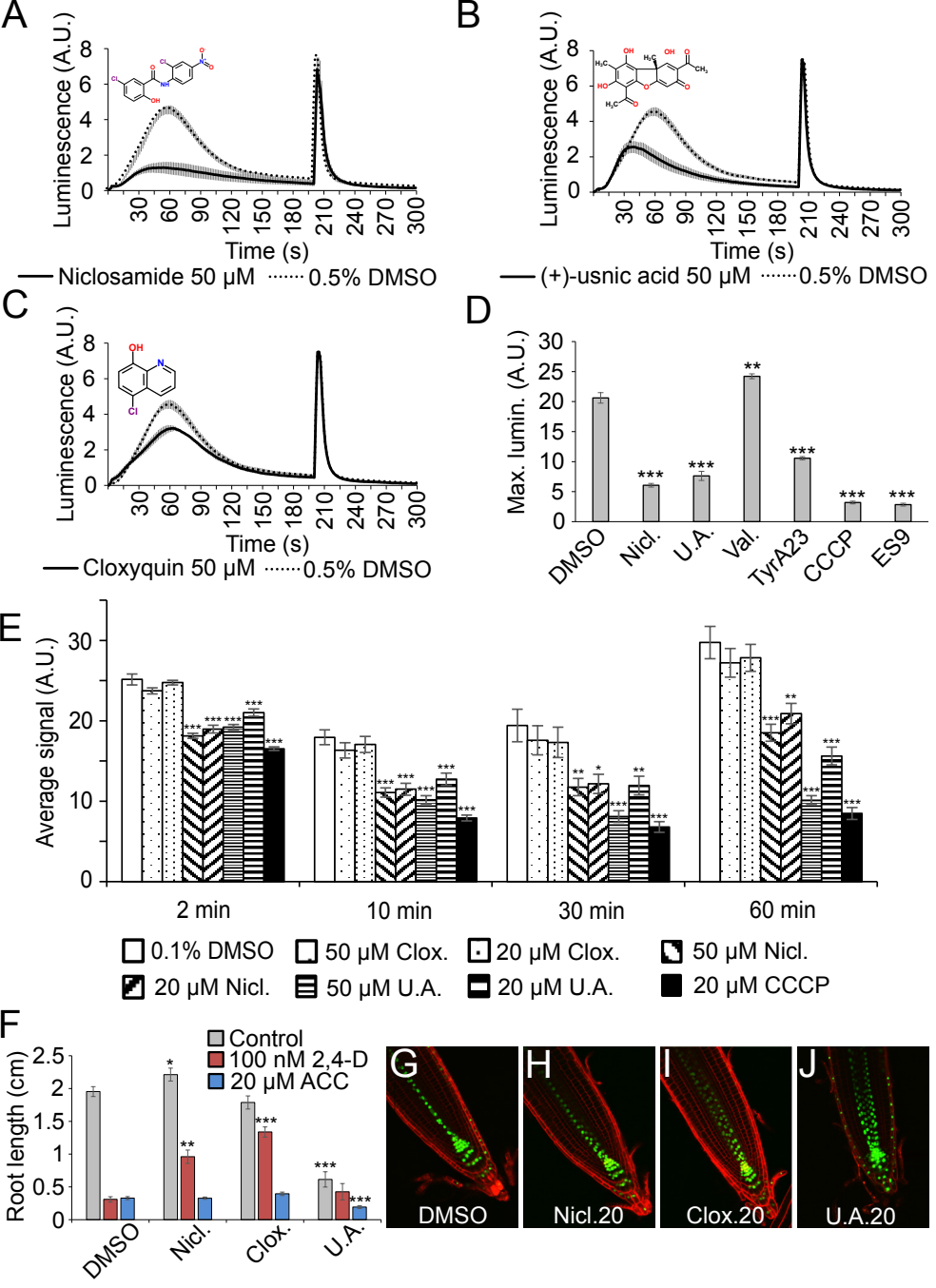

Fig. 5. Protonophores impair the 2,4-D-induced Ca^{2+} response, and render roots insensitive to 2,4-D. (A-C) 2,4-D-induced Ca^{2+} response of YFP-apoaequorin-expressing BY-2 cells treated with 50 µM niclosamide **(A),** (+)-usnic acid **(B)** or cloxyquin **(C)**. Discharge solution was added after 200 seconds. The data is represented by average luminescence values of 4 individual measurements (solid lines) in comparison to the average of 4 DMSO controls (dotted lines) in the same multi-well plate. Error bars represent ± SEM. **(D)** Maximum 2,4-D-induced luminescence in YFP-apoaequorin-expressing BY-2 cells treated with 50 µM of the hit protonophores niclosamide and (+)-usnic acid, the ionophore valinomycin, or the non-hit protonophores tyrphostin A23, CCCP and ES9. Four individual measurements were performed for each treatment and compared to the average of 8 DMSO controls in the same multi-well plate. Error bars represent ± SEM. Student's t-test p-values: **p < 0.01, ***p < 0.001. **(E)** ATP measurements of BY-2 cells pre-treated with 0.5% DMSO (white), 20 µM CCCP (black), or 20 µM or 50 µM of cloxyquin (dots), niclosamide (diagonal stripes) or (+)-usnic acid (horizontal stripes), respectively. ATP was measured 2, 10, 30 and 60 minutes after compound treatment. Error bars represent ± SEM. Student's t-test p-values: *p < 0.05, **p < 0.01, ***p < 0.001. **(F)** Average primary root length of WT Col-0 seedlings grown for 7 days on ½ MS medium in presence of 0.1% DMSO or 20 µM niclosamide, cloxyquin or (+)-usnic acid (grey bars), and supplemented with 100 nM 2,4-D (red bars) or 20 µM ACC (blue bars). Root lengths represented as average of 12-21 roots. Error bars represent ± SEM. Student's t-test p-values: *p < 0.05, **p < 0.01, ***p < 0.001. **(G-J)** Confocal microscopic images of 5-day-old DR5rev::VENUS-N7 seedlings grown on 0.1% DMSO **(G)**, 20 µM niclosamide **(H)**, 20 µM cloxyquin **(I)** or 20 µM (+)-usnic acid **(J)**, respectively. Green: DR5rev::VENUS-N7 signal; Red: propidium iodide staining. The image in **(G)** is identical to Fig. 3F.

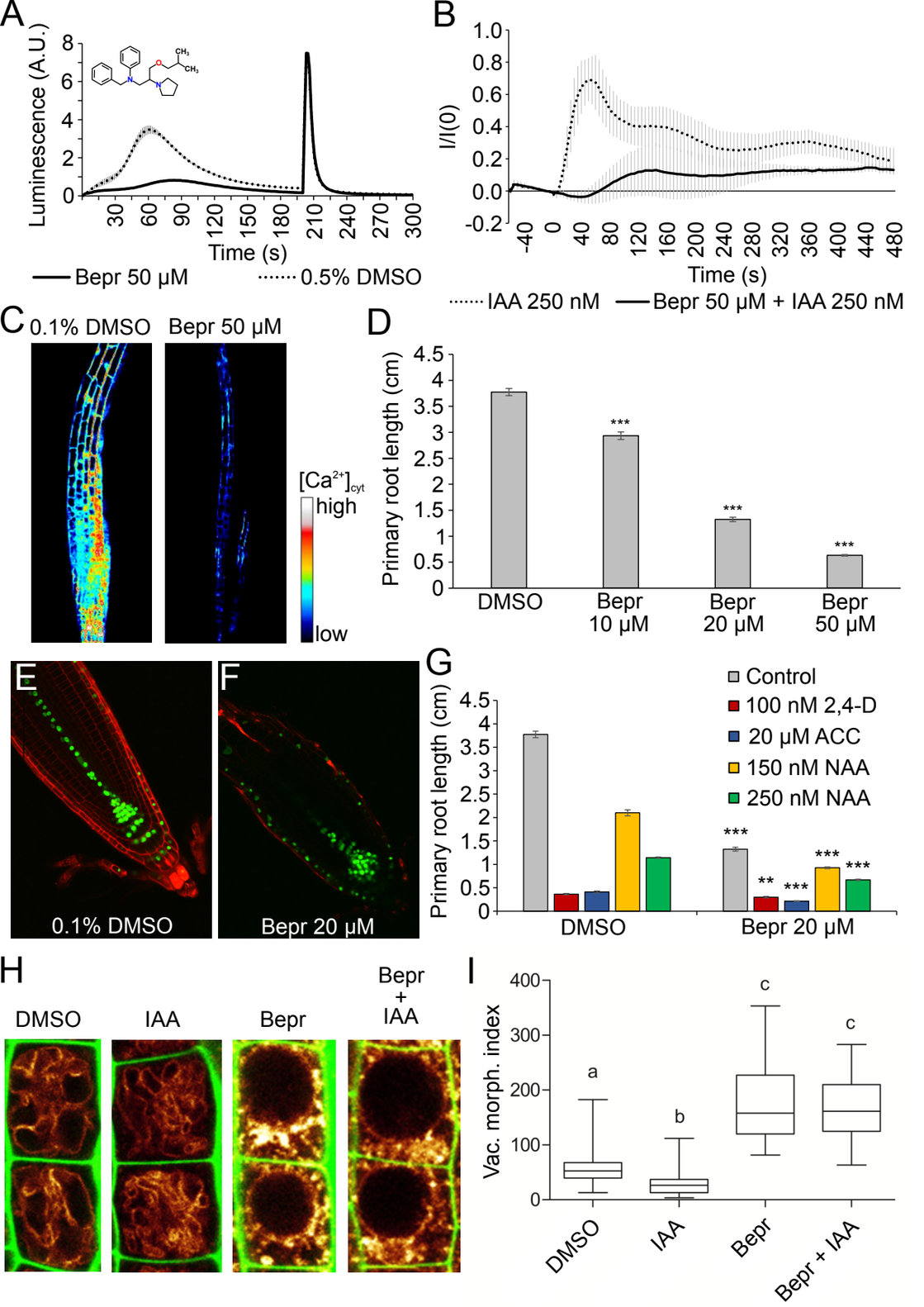

Fig. 6. Bepridil is a potent inhibitor of auxin-induced Ca^{2+} signaling. (A) 2,4-D-induced Ca^{2+} response of YFP-apoaequorin-expressing BY-2 cells treated with 50 µM bepridil. Discharge solution was added after 200 seconds. The data is represented by average luminescence values of 4 individual measurements (solid lines) in comparison to the average of 4 DMSO controls (dotted lines) in the same multi-well plate. Error bars represent ± SEM. **(B)** Fluorescent intensity in R-GECO1-expressing *Arabidopsis* seedlings after IAA treatment. Seedlings were pre-treated for 30 minutes with 50 µM bepridil (solid lines) or 0.1% DMSO (dotted lines). IAA (250 nM) was added at time point 0, and R-GECO1 fluorescence intensity was monitored for 8 minutes. The data is represented by average fluorescence values of 4 individual measurements in comparison to the average of 3 DMSO controls. Error bars represent ± SEM. **(C)** Snapshot of the peak Ca^{2+} signal elicited in R-GECO1 seedlings by 250 nM IAA after a 30 minute pre-treatment with 0.1% DMSO (left) or 50 µM bepridil (right), respectively. The snapshot was taken 30 seconds after IAA addition. **(D)** Average primary root length of WT Col-0 seedlings grown for 7 days on ½ MS medium in presence of 0.1% DMSO or 10 µM, 20 µM or 50 µM of bepridil, respectively. Root lengths represented as average of 54-60 roots. Error bars represent ± SEM. Student's t-test p-values: ***$p < 0.001$. **(E-F)** Confocal microscopic images of 5 day old DR5rev::VENUS-N7 seedlings grown on 0.1% DMSO **(E)** and 20 µM bepridil **(F)**, respectively. Green: DR5rev::VENUS-N7 signal; Red: propidium iodide staining. **(G)** Average primary root length of WT *Arabidopsis thaliana* seedlings grown for 7 days on ½ MS medium in presence of 20 µM bepridil or 0.1% DMSO (grey), and supplemented with 100 nM 2,4-D (red), 20 µM ACC (blue), 150 nM NAA (yellow) or 250 nM NAA (green). Root lengths represented as average of 51-61 roots. Error bars represent ± SEM. Student's t-test p-values in comparison to DMSO: **$p < 0.01$, ***$p < 0.001$. **(H-I)** The effect of bepridil on vacuolar morphology. Six-day old pUBQ10::VAMP711-YFP seedlings were pre-treated with 50 µM bepridil or solvent control for 5 h, followed by 3-h treatments with (DMSO), 250 nM IAA (IAA), 50 µM bepridil (Bepr) or 50 µM bepridil and 250 nM IAA (Bepr + IAA). Tonoplast localized VAMP711-YFP (orange) as vacuolar marker and propidium iodide stain (green) for decorating the cell wall were used for confocal imaging of atrichoblast cells **(H)**. The quantification of the vacuolar morphology index was performed with 4 vacuoles of late meristematic atrichoblasts per root, with 10-14 roots used for each treatment **(I)**. Statistical analysis was performed using one-way Anova (Kruskal-Wallis test) followed by Dunn´s multiple comparison test, b: $p < 0.05$, c: $p < 0.001$.

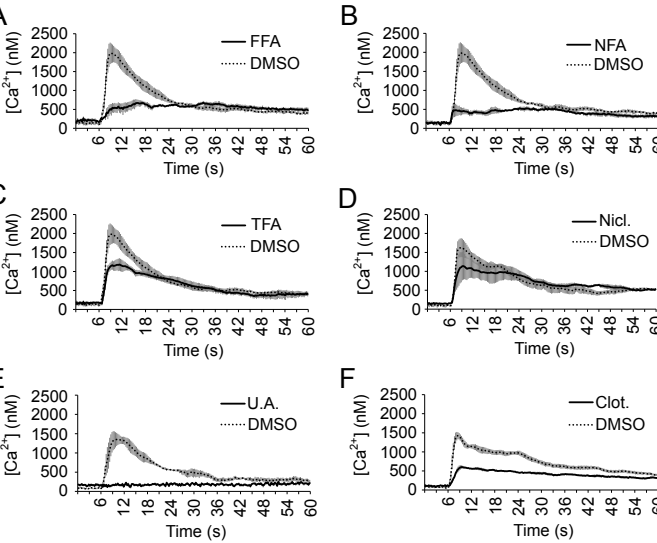

Fig. 7. Sucrose-induced Ca^{2+} signals are highly sensitive to fenamates, protonophores and imidazoles. (A-H) Sucrose-induced Ca^{2+} responses of YFP-apoaequorin-expressing *Arabidopsis thaliana* seedlings treated with fenamates **(A-C)**, protonophores **(D-E)**, imidazoles **(F-G)**, or bepridil **(H)**. The data is represented by average luminescence values of 4 individual measurements (solid lines) in comparison to the average of 4 DMSO controls (dotted lines) in the same multi-well plate. Error bars represent ± SEM. FFA, flufenamic acid; NFA, niflumic acid; TFA, tolfenamic acid; Nicl., niclosamide; U.A., (+)-usnic acid; Clot., clotrimazole; Ox. Nit., oxiconazole nitrate; Bepr., bepridil.

Parsed Citations

Ali A, Jadhav A, Jangid P, Patil R, Shelar A, Karuppayil SM (2018) The human muscarinic acetylcholine receptor antagonist, Dicyclomine targets signal transduction genes and inhibits the virulence factors in the human pathogen, Candida albicans. J Antibiot (Tokyo) 71: 456-466

Pubmed: Author and Title
Google Scholar: Author Only Title Only Author and Title

Ane JM, Kiss GB, Riely BK, Penmetsa RV, Oldroyd GE, Ayax C, Levy J, Debelle F, Baek JM, Kalo P, Rosenberg C, Roe BA, Long SR, Denarie J, Cook DR (2004) Medicago truncatula DMI1 required for bacterial and fungal symbioses in legumes. Science 303: 1364-1367

Pubmed: Author and Title
Google Scholar: Author Only Title Only Author and Title

Barbez E, Dünser K, Gaidora A, Lendl T, Busch W (2017) Auxin steers root cell expansion via apoplastic pH regulation in Arabidopsis thaliana. Proc Natl Acad Sci U S A 114: E4884-E4893

Pubmed: Author and Title
Google Scholar: Author Only Title Only Author and Title

Behera S, Xu Z, Luoni L, Bonza MC, Doccula FG, De Michelis MI, Morris RJ, Schwarzlander M, Costa A (2018) Cellular Ca(2+) Signals Generate Defined pH Signatures in Plants. The Plant cell 30: 2704-2719

Pubmed: Author and Title
Google Scholar: Author Only Title Only Author and Title

Benjamins R, Ampudia CSG, Hooykaas PJJ, Offringa R (2003) PINOID-mediated signaling involves calcium-binding proteins. Plant Physiology 132: 1623-1630

Pubmed: Author and Title
Google Scholar: Author Only Title Only Author and Title

Chaiwanon J, Wang W, Zhu JY, Oh E, Wang ZY (2016) Information Integration and Communication in Plant Growth Regulation. Cell 164: 1257-1268

Pubmed: Author and Title
Google Scholar: Author Only Title Only Author and Title

Charpentier M, Bredemeier R, Wanner G, Takeda N, Schleiff E, Parniske M (2008) Lotus japonicus CASTOR and POLLUX are ion channels essential for perinuclear calcium spiking in legume root endosymbiosis. Plant Cell 20: 3467-3479

Pubmed: Author and Title
Google Scholar: Author Only Title Only Author and Title

Charpentier M, Sun J, Vaz Martins T, Radhakrishnan GV, Findlay K, Soumpourou E, Thouin J, Very AA, Sanders D, Morris RJ, Oldroyd GE (2016) Nuclear-localized cyclic nucleotide-gated channels mediate symbiotic calcium oscillations. Science 352: 1102-1105

Pubmed: Author and Title
Google Scholar: Author Only Title Only Author and Title

Clough SJ, Bent AF (1998) Floral dip: a simplified method for Agrobacterium-mediated transformation of Arabidopsis thaliana. The Plant journal : for cell and molecular biology 16: 735-743

Pubmed: Author and Title
Google Scholar: Author Only Title Only Author and Title

De Vriese K, Costa A, Beeckman T, Vanneste S (2018) Pharmacological Strategies for Manipulating Plant Ca(2+) Signalling. Int J Mol Sci 19

Pubmed: Author and Title
Google Scholar: Author Only Title Only Author and Title

Dejonghe W, Kuenen S, Mylle E, Vasileva M, Keech O, Viotti C, Swerts J, Fendrych M, Ortiz-Morea FA, Mishev K, Delang S, Scholl S, Zarza X, Heilmann M, Kourelis J, Kasprowicz J, Nguyen le SL, Drozdzecki A, Van Houtte I, Szatmari AM, Majda M, Baisa G, Bednarek SY, Robert S, Audenaert D, Testerink C, Munnik T, Van Damme D, Heilmann I, Schumacher K, Winne J, Friml J, Verstreken P, Russinova E (2016) Mitochondrial uncouplers inhibit clathrin-mediated endocytosis largely through cytoplasmic acidification. Nat Commun 7: 11710

Pubmed: Author and Title
Google Scholar: Author Only Title Only Author and Title

Dela Fuente RK, Leopold AC (1973) A role for calcium in auxin transport. Plant Physiol 51: 845-847

Pubmed: Author and Title
Google Scholar: Author Only Title Only Author and Title

Diatloff E, Roberts M, Sanders D, Roberts SK (2004) Characterization of anion channels in the plasma membrane of Arabidopsis epidermal root cells and the identification of a citrate-permeable channel induced by phosphate starvation. Plant Physiol 136: 4136-4149

Pubmed: Author and Title
Google Scholar: Author Only Title Only Author and Title

Dindas J, Scherzer S, Roelfsema MRG, von Meyer K, Muller HM, Al-Rasheid KAS, Palme K, Dietrich P, Becker D, Bennett MJ, Hedrich R (2018) AUX1-mediated root hair auxin influx governs SCF(TIR1/AFB)-type Ca(2+) signaling. Nat Commun 9: 1174

Pubmed: Author and Title
Google Scholar: Author Only Title Only Author and Title

Dünser K, Gupta S, Ringli C, Kleine-Vehn J (2017) LRX- and FER-dependent extracellular sensing coordinates vacuolar size for cytosol homeostasis. bioRxiv. Preprint, posted December 8, 2017.
Pubmed: Author and Title
Google Scholar: Author Only Title Only Author and Title

Ebine K, Okatani Y, Uemura T, Goh T, Shoda K, Niihama M, Morita MT, Spitzer C, Otegui MS, Nakano A, Ueda T (2008) A SNARE complex unique to seed plants is required for protein storage vacuole biogenesis and seed development of Arabidopsis thaliana. Plant Cell 20: 3006-3021
Pubmed: Author and Title
Google Scholar: Author Only Title Only Author and Title

Edel KH, Marchadier E, Brownlee C, Kudla J, Hetherington AM (2017) The Evolution of Calcium-Based Signalling in Plants. Current biology : CB 27: R667-R679
Pubmed: Author and Title
Google Scholar: Author Only Title Only Author and Title

Fendrych M, Akhmanova M, Merrin J, Glanc M, Hagihara S, Takahashi K, Uchida N, Torii KU, Friml J (2018) Rapid and reversible root growth inhibition by TIR1 auxin signalling. Nat Plants 4: 453-459
Pubmed: Author and Title
Google Scholar: Author Only Title Only Author and Title

Forde BG, Roberts MR (2014) Glutamate receptor-like channels in plants: a role as amino acid sensors in plant defence? F1000prime reports 6: 37

Furuichi T, Mori IC, Takahashi K, Muto S (2001) Sugar-induced increase in cytosolic Ca(2+) in Arabidopsis thaliana whole plants. Plant Cell Physiol 42: 1149-1155
Pubmed: Author and Title
Google Scholar: Author Only Title Only Author and Title

Gao D, Knight MR, Trewavas AJ, Sattelmacher B, Plieth C (2004) Self-reporting Arabidopsis expressing pH and [Ca2+] indicators unveil ion dynamics in the cytoplasm and in the apoplast under abiotic stress. Plant physiology 134: 898-908
Pubmed: Author and Title
Google Scholar: Author Only Title Only Author and Title

Geldner N, Denervaud-Tendon V, Hyman DL, Mayer U, Stierhof YD, Chory J (2009) Rapid, combinatorial analysis of membrane compartments in intact plants with a multicolor marker set. Plant J 59: 169-178
Pubmed: Author and Title
Google Scholar: Author Only Title Only Author and Title

Gilliham M, Tester M (2005) The regulation of anion loading to the maize root xylem. Plant Physiol 137: 819-828
Pubmed: Author and Title
Google Scholar: Author Only Title Only Author and Title

Graham GG (2016) Fenamates. . Parnham M. (eds) Compendium of Inflammatory Diseases.
Pubmed: Author and Title
Google Scholar: Author Only Title Only Author and Title

Habjan S, Vandenberg RJ (2009) Modulation of glutamate and glycine transporters by niflumic, flufenamic and mefenamic acids. Neurochem Res 34: 1738-1747
Pubmed: Author and Title
Google Scholar: Author Only Title Only Author and Title

Heath RJ, Rubin JR, Holland DR, Zhang E, Snow ME, Rock CO (1999) Mechanism of triclosan inhibition of bacterial fatty acid synthesis. J Biol Chem 274: 11110-11114
Pubmed: Author and Title
Google Scholar: Author Only Title Only Author and Title

Heisler MG, Ohno C, Das P, Sieber P, Reddy GV, Long JA, Meyerowitz EM (2005) Patterns of auxin transport and gene expression during primordium development revealed by live imaging of the Arabidopsis inflorescence meristem. Curr Biol 15: 1899-1911
Pubmed: Author and Title
Google Scholar: Author Only Title Only Author and Title

Herrmann A, Felle HH (1995) Tip Growth in Root Hair-Cells of Sinapis-Alba L - Significance of Internal and External Ca2+ and Ph. New Phytologist 129: 523-533
Pubmed: Author and Title
Google Scholar: Author Only Title Only Author and Title

Himschoot E, Krebs M, Costa A, Beeckman T, Vanneste S (2018) Calcium Ion Dynamics in Roots: Imaging and Analysis. Methods Mol Biol 1761: 115-130
Pubmed: Author and Title
Google Scholar: Author Only Title Only Author and Title

Hogg RC, Wang Q, Large WA (1994) Action of niflumic acid on evoked and spontaneous calcium-activated chloride and potassium currents in smooth muscle cells from rabbit portal vein. Br J Pharmacol 112: 977-984
Pubmed: Author and Title
Google Scholar: Author Only Title Only Author and Title

Hongmanee P, Rukseree K, Buabut B, Somsri B, Palittapongarnpim P (2007) In vitro activities of cloxyquin (5-chloroquinolin-8-ol) against Mycobacterium tuberculosis. Antimicrob Agents Chemother 51: 1105-1106
Pubmed: Author and Title
Google Scholar: Author Only Title Only Author and Title

Isenburg JC, Simionescu DT, Vyavahare NR (2005) Tannic acid treatment enhances biostability and reduces calcification of glutaraldehyde fixed aortic wall. Biomaterials 26: 1237-1245
Pubmed: Author and Title
Google Scholar: Author Only Title Only Author and Title

Jegasothy BV, Pakes GE (1991) Oxiconazole nitrate: pharmacology, efficacy, and safety of a new imidazole antifungal agent. Clin Ther 13: 126-141
Pubmed: Author and Title
Google Scholar: Author Only Title Only Author and Title

Jia T, Gao C, Cui Y, Wang J, Ding Y, Cai Y, Ueda T, Nakano A, Jiang L (2013) ARA7(Q69L) expression in transgenic Arabidopsis cells induces the formation of enlarged multivesicular bodies. J Exp Bot 64: 2817-2829
Pubmed: Author and Title
Google Scholar: Author Only Title Only Author and Title

Keinath NF, Waadt R, Brugman R, Schroeder JI, Grossmann G, Schumacher K, Krebs M (2015) Live Cell Imaging with R-GECO1 Sheds Light on flg22- and Chitin-Induced Transient [Ca(2+)]cyt Patterns in Arabidopsis. Mol Plant 8: 1188-1200
Pubmed: Author and Title
Google Scholar: Author Only Title Only Author and Title

Knight H, Trewavas AJ, Knight MR (1996) Cold calcium signaling in Arabidopsis involves two cellular pools and a change in calcium signature after acclimation. Plant Cell 8: 489-503
Pubmed: Author and Title
Google Scholar: Author Only Title Only Author and Title

Knight MR, Campbell AK, Smith SM, Trewavas AJ (1991) Transgenic plant aequorin reports the effects of touch and cold-shock and elicitors on cytoplasmic calcium. Nature 352: 524-526
Pubmed: Author and Title
Google Scholar: Author Only Title Only Author and Title

Korade Z, Kim HY, Tallman KA, Liu W, Koczok K, Balogh I, Xu L, Mirnics K, Porter NA (2016) The Effect of Small Molecules on Sterol Homeostasis: Measuring 7-Dehydrocholesterol in Dhcr7-Deficient Neuro2a Cells and Human Fibroblasts. J Med Chem 59: 1102-1115
Pubmed: Author and Title
Google Scholar: Author Only Title Only Author and Title

Kudla J, Batistic O, Hashimoto K (2010) Calcium signals: the lead currency of plant information processing. Plant Cell 22: 541-563
Pubmed: Author and Title
Google Scholar: Author Only Title Only Author and Title

Kudla J, Becker D, Grill E, Hedrich R, Hippler M, Kummer U, Parniske M, Romeis T, Schumacher K (2018) Advances and current challenges in calcium signaling. The New phytologist 218: 414-431
Pubmed: Author and Title
Google Scholar: Author Only Title Only Author and Title

Lanner JT, Georgiou DK, Joshi AD, Hamilton SL (2010) Ryanodine receptors: structure, expression, molecular details, and function in calcium release. Cold Spring Harbor perspectives in biology 2: a003996
Pubmed: Author and Title
Google Scholar: Author Only Title Only Author and Title

Latkowska E, Lechowski Z, Bialczyk J, Pilarski J (2006) Photosynthesis and water relations in tomato plants cultivated long-term in media containing (+)-usnic acid. J Chem Ecol 32: 2053-2066
Pubmed: Author and Title
Google Scholar: Author Only Title Only Author and Title

Lavy M, Estelle M (2016) Mechanisms of auxin signaling. Development 143: 3226-3229
Pubmed: Author and Title
Google Scholar: Author Only Title Only Author and Title

Lipsanen A, Flunkert S, Kuptsova K, Hiltunen M, Windisch M, Hutter-Paier B, Jolkkonen J (2013) Non-selective calcium channel blocker bepridil decreases secondary pathology in mice after photothrombotic cortical lesion. PLoS One 8: e60235
Pubmed: Author and Title
Google Scholar: Author Only Title Only Author and Title

Liu J, Moore S, Chen C, Lindsey K (2017) Crosstalk Complexities between Auxin, Cytokinin, and Ethylene in Arabidopsis Root Development: From Experiments to Systems Modeling, and Back Again. Molecular plant 10: 1480-1496

Pubmed: Author and Title
Google Scholar: Author Only Title Only Author and Title

Lofke C, Dunser K, Scheuring D, Kleine-Vehn J (2015) Auxin regulates SNARE-dependent vacuolar morphology restricting cell size. Elife 4

Pubmed: Author and Title
Google Scholar: Author Only Title Only Author and Title

Ma W, Berkowitz GA (2011) Ca2+ conduction by plant cyclic nucleotide gated channels and associated signaling components in pathogen defense signal transduction cascades. The New phytologist 190: 566-572

Pubmed: Author and Title
Google Scholar: Author Only Title Only Author and Title

Mehlmer N, Parvin N, Hurst CH, Knight MR, Teige M, Vothknecht UC (2012) A toolset of aequorin expression vectors for in planta studies of subcellular calcium concentrations in Arabidopsis thaliana. J Exp Bot 63: 1751-1761

Pubmed: Author and Title
Google Scholar: Author Only Title Only Author and Title

Michard E, Simon AA, Tavares B, Wudick MM, Feijo JA (2017) Signaling with Ions: The Keystone for Apical Cell Growth and Morphogenesis in Pollen Tubes. Plant Physiology 173: 91-111

Pubmed: Author and Title
Google Scholar: Author Only Title Only Author and Title

Monin MB, Krause P, Stelling R, Bocuk D, Niebert S, Klemm F, Pukrop T, Koenig S (2016) The anthelmintic niclosamide inhibits colorectal cancer cell lines via modulation of the canonical and noncanonical Wnt signaling pathway. J Surg Res 203: 193-205

Pubmed: Author and Title
Google Scholar: Author Only Title Only Author and Title

Monshausen GB, Bibikova TN, Weisenseel MH, Gilroy S (2009) Ca2+ regulates reactive oxygen species production and pH during mechanosensing in Arabidopsis roots. The Plant cell 21: 2341-2356

Pubmed: Author and Title
Google Scholar: Author Only Title Only Author and Title

Monshausen GB, Messerli MA, Gilroy S (2008) Imaging of the Yellow Cameleon 3.6 indicator reveals that elevations in cytosolic Ca(2+) follow oscillating increases in growth in root hairs of arabidopsis. Plant Physiology 147: 1690-1698

Pubmed: Author and Title
Google Scholar: Author Only Title Only Author and Title

Murthy SE, Dubin AE, Whitwam T, Jojoa-Cruz S, Cahalan SM, Mousavi SAR, Ward AB, Patapoutian A (2018) OSCA/TMEM63 are an Evolutionarily Conserved Family of Mechanically Activated Ion Channels. eLife 7

Pubmed: Author and Title
Google Scholar: Author Only Title Only Author and Title

Nagata T, Iizumi S, Satoh K, Ooka H, Kawai J, Carninci P, Hayashizaki Y, Otomo Y, Murakami K, Matsubara K, Kikuchi S (2004) Comparative analysis of plant and animal calcium signal transduction element using plant full-length cDNA data. Molecular biology and evolution 21: 1855-1870

Pubmed: Author and Title
Google Scholar: Author Only Title Only Author and Title

Narahara KA, Singh BN, Karliner JS, Corday SR, Hossack KF (1992) Bepridil hydrochloride compared with placebo in patients with stable angina pectoris. Am J Cardiol 69: 37D-42D

Pubmed: Author and Title
Google Scholar: Author Only Title Only Author and Title

Nixon GF, Mignery GA, Somlyo AV (1994) Immunogold localization of inositol 1,4,5-trisphosphate receptors and characterization of ultrastructural features of the sarcoplasmic reticulum in phasic and tonic smooth muscle. Journal of muscle research and cell motility 15: 682-700

Pubmed: Author and Title
Google Scholar: Author Only Title Only Author and Title

Pentikainen PJ, Neuvonen PJ, Backman C (1981) Human pharmacokinetics of tolfenamic acid, a new anti-inflammatory agent. Eur J Clin Pharmacol 19: 359-365

Pubmed: Author and Title
Google Scholar: Author Only Title Only Author and Title

Philippar K, Ivashikina N, Ache P, Christian M, Luthen H, Palme K, Hedrich R (2004) Auxin activates KAT1 and KAT2, two K+-channel genes expressed in seedlings of Arabidopsis thaliana. Plant J 37: 815-827

Pubmed: Author and Title
Google Scholar: Author Only Title Only Author and Title

Qiu W, Ren B, Dai H, Zhang L, Zhang Q, Zhou X, Li Y (2017) Clotrimazole and econazole inhibit Streptococcus mutans biofilm and virulence in vitro. Arch Oral Biol 73: 113-120

Pubmed: Author and Title
Google Scholar: Author Only Title Only Author and Title

Rigo G, Ayaydin F, Tietz O, Zsigmond L, Kovacs H, Pay A, Salchert K, Darula Z, Medzihradszky KF, Szabados L, Palme K, Koncz C, Cseplo A (2013) Inactivation of plasma membrane-localized CDPK-RELATED KINASE5 decelerates PIN2 exocytosis and root gravitropic response in Arabidopsis. The Plant cell 25: 1592-1608
Pubmed: Author and Title
Google Scholar: Author Only Title Only Author and Title

Sarajarvi T, Lipsanen A, Makinen P, Peraniemi S, Soininen H, Haapasalo A, Jolkkonen J, Hiltunen M (2012) Bepridil decreases Abeta and calcium levels in the thalamus after middle cerebral artery occlusion in rats. J Cell Mol Med 16: 2754-2767
Pubmed: Author and Title
Google Scholar: Author Only Title Only Author and Title

Scheuring D, Lofke C, Kruger F, Kittelmann M, Eisa A, Hughes L, Smith RS, Hawes C, Schumacher K, Kleine-Vehn J (2016) Actin-dependent vacuolar occupancy of the cell determines auxin-induced growth repression. Proceedings of the National Academy of Sciences of the United States of America 113: 452-457
Pubmed: Author and Title
Google Scholar: Author Only Title Only Author and Title

Schindelin J, Arganda-Carreras I, Frise E, Kaynig V, Longair M, Pietzsch T, Preibisch S, Rueden C, Saalfeld S, Schmid B, Tinevez JY, White DJ, Hartenstein V, Eliceiri K, Tomancak P, Cardona A (2012) Fiji: an open-source platform for biological-image analysis. Nat Methods 9: 676-682
Pubmed: Author and Title
Google Scholar: Author Only Title Only Author and Title

Shih HW, DePew CL, Miller ND, Monshausen GB (2015) The Cyclic Nucleotide-Gated Channel CNGC14 Regulates Root Gravitropism in Arabidopsis thaliana. Curr Biol 25: 3119-3125
Pubmed: Author and Title
Google Scholar: Author Only Title Only Author and Title

Shimomura O (2005) The discovery of aequorin and green fluorescent protein. Journal of microscopy 217: 1-15
Pubmed: Author and Title
Google Scholar: Author Only Title Only Author and Title

Shimomura O, Johnson FH, Saiga Y (1962) Extraction, purification and properties of aequorin, a bioluminescent protein from the luminous hydromedusan, Aequorea. J Cell Comp Physiol 59: 223-239
Pubmed: Author and Title
Google Scholar: Author Only Title Only Author and Title

Stephan AB, Kunz HH, Yang E, Schroeder JI (2016) Rapid hyperosmotic-induced Ca2+ responses in Arabidopsis thaliana exhibit sensory potentiation and involvement of plastidial KEA transporters. Proc Natl Acad Sci U S A 113: E5242-5249
Pubmed: Author and Title
Google Scholar: Author Only Title Only Author and Title

Swarup R, Friml J, Marchant A, Ljung K, Sandberg G, Palme K, Bennett M (2001) Localization of the auxin permease AUX1 suggests two functionally distinct hormone transport pathways operate in the Arabidopsis root apex. Genes & development 15: 2648-2653
Pubmed: Author and Title
Google Scholar: Author Only Title Only Author and Title

Thiel G, Weise R (1999) Auxin augments conductance of K+ inward rectifier in maize coleoptile protoplasts. Planta 208: 38-45
Pubmed: Author and Title
Google Scholar: Author Only Title Only Author and Title

Thomine S, Zimmerman S, Van Duijn B, Barbier-Brygoo H, Guern J (1994) Calcium channel antagonists induce direct inhibition of the outward rectifying potassium channel in tobacco protoplasts. FEBS Lett 340: 45-50
Pubmed: Author and Title
Google Scholar: Author Only Title Only Author and Title

Tuteja N, Mahajan S (2007) Calcium signaling network in plants: an overview. Plant Signal Behav 2: 79-85
Pubmed: Author and Title
Google Scholar: Author Only Title Only Author and Title

Vanneste S, Friml J (2009) Auxin: a trigger for change in plant development. Cell 136: 1005-1016
Pubmed: Author and Title
Google Scholar: Author Only Title Only Author and Title

Vermeer JE, van Leeuwen W, Tobena-Santamaria R, Laxalt AM, Jones DR, Divecha N, Gadella TW, Jr., Munnik T (2006) Visualization of PtdIns3P dynamics in living plant cells. The Plant journal : for cell and molecular biology 47: 687-700
Pubmed: Author and Title
Google Scholar: Author Only Title Only Author and Title

Weijers D, Wagner D (2016) Transcriptional Responses to the Auxin Hormone. Annual review of plant biology 67: 539-574
Pubmed: Author and Title
Google Scholar: Author Only Title Only Author and Title

Yang Y, Hammes UZ, Taylor CG, Schachtman DP, Nielsen E (2006) High-affinity auxin transport by the AUX1 influx carrier protein. Current biology : CB 16: 1123-1127

Pubmed: Author and Title
Google Scholar: Author Only Title Only Author and Title

Yatani A, Brown AM, Schwartz A (1986) Bepridil block of cardiac calcium and sodium channels. J Pharmacol Exp Ther 237: 9-17
Pubmed: Author and Title
Google Scholar: Author Only Title Only Author and Title

Yuan F, Yang H, Xue Y, Kong D, Ye R, Li C, Zhang J, Theprungsirikul L, Shrift T, Krichilsky B, Johnson DM, Swift GB, He Y, Siedow JN, Pei ZM (2014) OSCA1 mediates osmotic-stress-evoked Ca2+ increases vital for osmosensing in Arabidopsis. Nature 514: 367-371
Pubmed: Author and Title
Google Scholar: Author Only Title Only Author and Title

Zhang J, Vanneste S, Brewer PB, Michniewicz M, Grones P, Kleine-Vehn J, Lofke C, Teichmann T, Bielach A, Cannoot B, Hoyerova K, Chen X, Xue HW, Benkova E, Zazimalova E, Friml J (2011) Inositol trisphosphate-induced Ca2+ signaling modulates auxin transport and PIN polarity. Dev Cell 20: 855-866
Pubmed: Author and Title
Google Scholar: Author Only Title Only Author and Title

Zhang JH, Chung TD, Oldenburg KR (1999) A Simple Statistical Parameter for Use in Evaluation and Validation of High Throughput Screening Assays. Journal of biomolecular screening 4: 67-73
Pubmed: Author and Title
Google Scholar: Author Only Title Only Author and Title

Zhang M, Wang D, Kang Y, Wu JX, Yao F, Pan C, Yan Z, Song C, Chen L (2018) Structure of the mechanosensitive OSCA channels. Nature structural & molecular biology 25: 850-858
Pubmed: Author and Title
Google Scholar: Author Only Title Only Author and Title

Zuccotti A, Clementi S, Reinbothe T, Torrente A, Vandael DH, Pirone A (2011) Structural and functional differences between L-type calcium channels: crucial issues for future selective targeting. Trends in pharmacological sciences 32: 366-375
Pubmed: Author and Title
Google Scholar: Author Only Title Only Author and Title